The Astronomical Journal, 125:208–223, 2003 January


# PHOTOMETRY OF THE GLOBULAR CLUSTER NGC 3201 AND ITS VARIABLE STARS

Andrew C. Layden
Department of Physics and Astronomy, 104 Overman Hall, Bowling Green State University, Bowling Green, OH 43403;
layden@baade.bgsu.edu

and

Ata Sarajedini
Department of Astronomy, 211 Bryant Space Science Center, University of Florida, Gainsville, FL 32611-2055;
ata@astro.ufl.edu
*Received 2002 September 3; accepted 2002 September 24*

## ABSTRACT

We present time series *BVI* photometry of the brighter stars in the halo globular cluster NGC 3201. We derive high-quality light curves for 58 RR Lyrae stars, all of which appear to be members of the cluster. We determine the foreground reddening of each RR Lyrae star from the star's color and confirm that the reddening varies significantly across the face of the cluster. We obtain a mean value of $E(B-V) = 0.25 \pm 0.02$ mag for stars within 2.′0 of the cluster center. Using the reddening values of the individual RR Lyrae stars, we made dereddened color-magnitude diagrams that reach from the red giant branch tip to ~2 mag below the main-sequence turnoff. Analysis of these diagrams indicates that NGC 3201 has an age of 13–14 Gyr, typical of other globular clusters of its metallicity. We detect low-level brightness variations in most of the cluster's brighter red giant stars and tentatively associate this variation with the small-amplitude red variables seen in the field. We also discovered several $\delta$ Scuti variable candidates, two of which appear to be cluster members. The distances derived from the $\delta$ Scuti and RR Lyrae stars are in good agreement, indicating $d = 4.7 \pm 0.2$ kpc.

*Key words:* color-magnitude diagrams — $\delta$ Scuti — dust, extinction — globular clusters: individual (NGC 3201) — RR Lyrae variable

*On-line material:* machine-readable tables

## 1. INTRODUCTION

RR Lyrae stars (RRLs) are an important standard candle for old stellar populations. They have been used to estimate distances to globular clusters, to the Galactic center, and to nearby galaxies within the Local Group. However, the absolute magnitude calibration, $M_V$(RR), remains uncertain at the 0.1 mag level and results of the various methods used to establish $M_V$(RR) span the uncomfortably large range of a quarter magnitude (Carretta et al. 2000). This uncertainty in distance is a major contributor to the uncertainty in the absolute ages of globular clusters (Chaboyer et al. 1998). Accurate cluster ages are critical to understanding the formation and early chemical enrichment of the Milky Way and to setting a hard observational limit on the age of the universe.

Fortunately, new distance estimates to nearby globular clusters gradually will become available, enabling a significant improvement in the $M_V$(RR) calibration. Following the work of Renzini et al. (1996) on NGC 6752 and of Cool, Piotto, & King (1996) on NGC 6397, the *Next Generation Space Telescope* should resolve white dwarf sequences in many nearby globular clusters. This will enable accurate distances to be obtained via comparisons with white dwarf cooling tracks and with nearby white dwarfs having trigonometric parallaxes. Not long after that, astrometric satellites such as NASA's *Space Interferometry Mission* and ESA's *GAIA* will measure direct trigonometric parallaxes for the globular clusters within ~10 kpc of the Sun (Unwin 2000; Perryman 2002).

To make the resulting $M_V$(RR) calibration as accurate as possible, high-quality time series photometry of the clusters' RRLs is required to provide apparent magnitudes averaged over the pulsation cycle of each RRL. The horizontal branches of the nearby globular clusters are bright (13 mag $< V_{HB} <$ 15 mag), making this a project for the smallest research-class telescopes available.

The globular NGC 3201 is a particularly appealing target. It is nearby ($V_{HB} = 14.8$ mag), rich in RRLs ($N_{RR} \approx 80$), and of Oosterhoff type I, so that the RRLs are minimally evolved off the zero-age horizontal branch. However, interstellar reddening presents a problem with NGC 3201. The Galactic coordinates ($l = 277.^{\circ}228$, $b = +8.^{\circ}461$) indicate a reddening of $E(B-V) \approx 0.25$ mag (Schlegel, Finkbeiner, & Davis 1998), and observations show the reddening to vary across the face of NGC 3201 (von Braun & Mateo 2001 and references therein). Fortunately, reddening estimates can be made directly from the RRLs themselves on a star-by-star basis from their observed colors (Sturch 1966; Blanco 1992).

In this paper, we lay the groundwork for these eventual $M_V$(RR) calibrations by presenting time series *BVI* photometry of the brighter stars in NGC 3201. In § 2 we discuss our observations and the photometric reductions. We then present color-magnitude diagrams of NGC 3201 that reach to $V \approx 19$ mag. Section 4 discusses the detection and the nature of the variable stars in NGC 3201. In § 5 we use the RRLs to derive the foreground reddening and present dereddened color-magnitude diagrams (CMDs) of the cluster stars. Using this information, we derive cluster properties including metallicity, distance, and age in § 6.

Piersimoni, Bono, & Ripepi (2002) recently published a paper that also presents time series *BVI* photometry of the RRLs in NGC 3201. It is worth noting some of the ways in which their paper differs from the present one. While their

*BVI* data are reassuringly similar to ours, their reddening analysis employed different calibrations and yielded somewhat different results from ours. Other points of interest in Piersimoni et al. (2002) included a detailed discussion of RRL amplitude modulation (the Blazhko effect) and an interesting comparison between the observed location of the RRLs in the CMD and the location predicted by theoretical models. By contrast, the present paper features, in addition to the RRL analysis, the detection and characterization of the other variable stars in NGC 3201, including a number of low-level variables on the red giant branch and several $\delta$ Scuti stars. In addition, we use the reddening and distance information derived from the RRL and $\delta$ Scuti stars to obtain an improved age estimate for NGC 3201.

## 2. OBSERVATIONS AND REDUCTIONS

### 2.1. *Observations*

Images of NGC 3201 were obtained in queue mode during 1999 February 2 through 21 with the YALO 1.0 m telescope at Cerro Tololo Inter-American Observatory. The ANDICAM camera was operated with one half of the Lick Loral 2048 × 2048 pixel CCD, giving a field of view of $5' \times 10'$. The cluster was visited 42 times during the run, with each visit consisting of three images (95 s in *B*, 40 s in *V*, and 35 s in *I*) centered east of the cluster center, plus three more images with the same filters and exposure times centered west of the cluster. The east and west regions overlapped by about $0'.5$, giving an effective field of $9'.5 \times 10'$ per visit.

Additional images were obtained during 2001 February 1 through March 14 with the YALO telescope and full-format ANDICAM CCD ($10' \times 10'$ field of view). The cluster was visited 27 times, with each visit consisting of several 70 s *I*-band images. In total, 50 images were obtained. The left-hand side of the CCD ($X < 1024$ pixels) had an elevated read noise. These observations were taken to support infrared *J*- and *K*-band photometry, which was obtained contemporaneously and which will be discussed in a separate paper.

The YALO telescope is queue scheduled, allowing us to acquire images spaced over a longer interval of time than is practical with traditional scheduling. This leads to more nearly complete phase coverage of the RR Lyrae light curves, particularly in cases for which the pulsation period is near the common values of 0.50 or 0.33 days. Observations were also made during periods of better seeing: the median seeing over our image set was $1''.4$. The images were processed by the YALO staff using standard techniques including overscan correction, bias subtraction, and flat-fielding using dome flats.

### 2.2. *Instrumental Photometry*

Initial photometry of each processed image was produced with DAOPHOT II (Stetson 1987). Stars were detected on each image with the FIND routine. About 300 bright isolated stars were then selected, and an initial point-spread function (PSF) was created from them. The PSF was allowed to vary with radial position on the image, and faint stars near PSF stars were iteratively subtracted from the image.

Lists of stellar coordinates from the 42 *V*-band frames, the 42 *B*-band frames, and the 42 *I*-band frames were matched using Stetson's DAOMASTER program, and ALLFRAME (Stetson 1994) was run separately on each stack of images. East and west regions were treated separately, as were the 50 *I*-band images obtained in 2001. The result is a final instrumental photometry list for each image.

### 2.3. *Standard Stars*

Observations of NGC 3201 were made during photometric conditions on five nights in 1999. In total, seven visits to NGC 3201 were made, with observations of Landolt (1992) standard stars taken before and after each cluster visit. The standards spanned a range in $B-V$ color from $-0.3$ to 1.3 mag, and ranged from 1.1 to 1.6 in air mass. Table 1 lists the UT dates of the photometric nights, the number of visits made to the cluster ($N_{\rm clus}$), and the number of visits made to separate standard fields ($N_{\rm fld}$) on each night. Aperture photometry of the Landolt standards was obtained with the DAOPHOT task PHOT implemented in IRAF.[1]

The resulting magnitudes are on an instrumental system and are corrected for the exposure time of each image. For each night, a least-squares fit was made separately for *B*-, *V*-, and *I*-band magnitudes by using an equation of the form

$$\psi - \Psi = c_0 + c_1 X + c_2 \gamma,$$

where $\psi$ and $\Psi$ are the aperture and standard magnitudes, respectively, and $X$ is the air mass. For the standard color, $\gamma$, we used $B-V$ for the *B*- and *V*-band data, and $V-I$ for the *I* band. The rms scatter about each fit is presented in Table 1, along with the number of points used in the fit. The small size of the scatter and the large number of standards obtained over many nights ensures an excellent photometric transformation for our data.

Observations of NGC 3201 made on these photometric nights were brought onto the standard systems as follows. A set of bright, relatively isolated stars was selected in the east and west fields. These stars were removed from the

[1] The Image Reduction and Analysis Facility (IRAF) is written and distributed by the National Optical Astronomy Observatories (NOAO).

TABLE 1
PHOTOMETRIC TRANSFORMATIONS

| Night | $N_{\rm clus}$ | $N_{\rm fld}$ | rms$_V$ | $N_V$ | rms$_B$ | $N_B$ | rms$_I$ | $N_I$ |
|---|---|---|---|---|---|---|---|---|
| 1999 Feb 8..... | 3 | 11 | 0.014 | 57 | 0.016 | 54 | 0.013 | 51 |
| 1999 Feb 15..... | 1 | 4 | 0.011 | 21 | 0.014 | 20 | 0.014 | 22 |
| 1999 Feb 16..... | 1 | 4 | 0.009 | 21 | 0.014 | 20 | 0.012 | 22 |
| 1999 Feb 18..... | 1 | 3 | 0.007 | 17 | 0.011 | 16 | 0.008 | 18 |
| 1999 Feb 20..... | 1 | 4 | 0.007 | 20 | 0.014 | 20 | 0.011 | 22 |

ALLFRAME star lists from each frame, and the resulting star list was subtracted from the corresponding image using the DAOPHOT II routine SUBSTAR, leaving only the bright stars on the frame. Aperture photometry was then performed on these stars in a manner identical with that used on the Landolt standards. The photometric transformations were applied, yielding magnitudes on the Johnson $B$ and $V$ and Kron-Cousins $I$ systems. Magnitudes from stars made during the seven photometric visits were then averaged. The result is a set of several hundred secondary standards spanning a large range in color and position across the NGC 3201 field.

### 2.4. *Final Photometry*

The ALLFRAME photometry from each of the 42 $B$, $V$, and $I$-band frames in the east field were then brought onto the standard system as follows. For a star to be included in the final list, it had to appear in at least eleven of the 42 frames for a given filter and in at least two of the three filters. The secondary standards were identified on each frame, and least-squares fits having the following form were performed:

$$\psi - \Psi = a_0 + a_1\gamma + a_2 X_{\rm pix} + a_3 Y_{\rm pix} + a_4 X_{\rm pix}^2 + a_5 X_{\rm pix} Y_{\rm pix} + a_6 Y_{\rm pix}^2 ,$$

where $\psi$ and $\Psi$ are the instrumental and standard magnitudes, respectively, the standard color, $\gamma$, is as defined in § 2.3, and $X_{\rm pix}$, $Y_{\rm pix}$ are the $X$ and $Y$ pixel coordinates. The position-dependent terms, which can reflect a position-dependent aperture correction, were always small and well behaved. The resulting transformation was then applied to all the stars on that image. The result is a photometry list for each image that is calibrated to the Landolt (1992) system.

These files were combined using DAOMASTER (Stetson 1994) to create a final photometry list containing positions and $B$, $V$, and $I$ magnitudes. Information from the east, west, and 2001 ($I$ band) data sets were merged during this procedure. Objects with extreme values of the DAOPHOT parameters "$\chi$" and "sharp" ($\Sigma$), which are generally galaxies or image defects (Stetson 1987), were then rejected. The resulting photometry for 10,944 stars is presented in Table 2.

We can compare our photometry on a star-by-star basis with the high-quality photometry of Stetson (2000), which is also calibrated to the Landolt (1992) system. Figure 1 shows the magnitude difference in each passband as a function of color. The agreement is quite good, although small zero-point offsets and color dependencies exist. Table 3 shows the statistical relation between our photometry and that of Stetson (2000), assuming a transformation of the form

$$\Psi_{\rm us} - \Psi_{\rm Stet} = a_0 + a_1(\gamma - 1.0) .$$

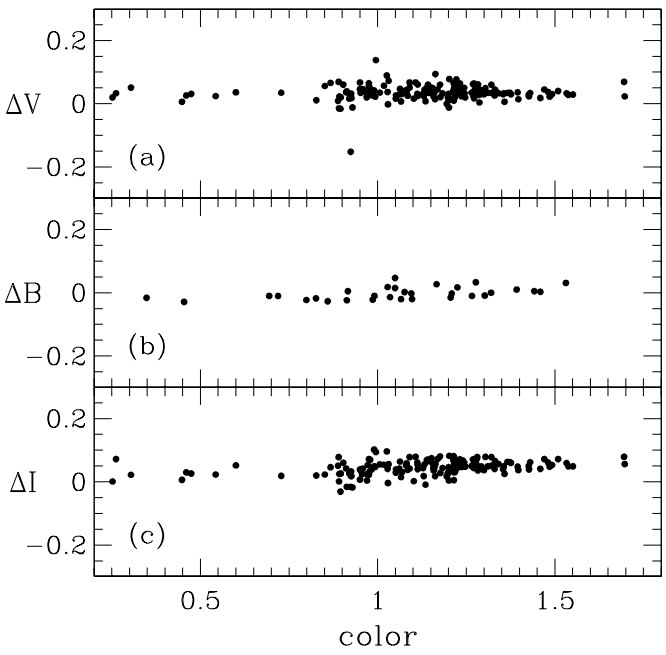


FIG. 1.—Comparison between our photometry and that of Stetson (2000). (*a*) $V_{\rm us}-V_{\rm Stet}$ as a function of $V-I$ color. (*b*) $B_{\rm us}-B_{\rm Stet}$ as a function of $B-V$ color. (*c*) $I_{\rm us}-I_{\rm Stet}$ as a function of $V-I$ color.

## 3. COLOR-MAGNITUDE DIAGRAMS

Figure 2 shows the CMDs of NGC 3201 by using the $BVI$ data from Table 2. Our data extend from the tip of the red giant branch (RGB) to below the main-sequence turnoff (MSTO) and sample the horizontal branch (HB) very well. The broad RGB is consistent with the variable reddening across the face of NGC 3201 noted by several authors (von Braun & Mateo 2001, and references therein). A population of blue straggler stars is seen above and blueward of the MSTO. We will use the properties of the RR Lyrae stars to map out and remove the reddening effects in § 5, and return to a discussion of the properties of NGC 3201 in § 6.

## 4. VARIABLE STARS

We searched for variable stars in our data set by looking for objects with large values of the variability index ($\Lambda$) computed in DAOMASTER (Stetson 1994). We found variable

TABLE 2
PHOTOMETRY OF NGC 3201 STARS

| ID | $X_{\rm pix}$ | $Y_{\rm pix}$ | $V$ | $\sigma_V$ | $B$ | $\sigma_B$ | $I$ | $\sigma_I$ | $\chi$ | $\Sigma$ |
|---|---|---|---|---|---|---|---|---|---|---|
| 1..... | 736.86 | 1268.73 | 11.781 | 0.001 | 13.352 | 0.001 | 10.164 | 0.001 | 1.269 | −0.065 |
| 2..... | 813.82 | 1175.30 | 11.812 | 0.001 | 13.617 | 0.001 | 10.015 | 0.001 | 1.346 | −0.084 |
| 3..... | 798.89 | 740.11 | 11.868 | 0.001 | 13.433 | 0.001 | 10.242 | 0.001 | 1.512 | −0.152 |
| 4..... | 271.33 | 984.05 | 11.895 | 0.001 | 13.536 | 0.001 | 10.226 | 0.001 | 1.091 | −0.071 |
| 5..... | 980.47 | 1509.81 | 12.072 | 0.001 | 13.607 | 0.001 | 10.497 | 0.001 | 1.177 | −0.047 |

NOTE.—Table 2 is presented in its entirety in the electronic edition of the Astronomical Journal. A portion is shown here for guidance regarding its form and content.

TABLE 3
PHOTOMETRIC COMPARISON WITH STETSON (2000)

| Filter | Color | $a_0$ | $a_1$ | rms | $N_{stars}$ |
|---|---|---|---|---|---|
| $V$..... | $V-I$ | +0.0346 | +0.0057 | 0.019 | 157 |
| $B$..... | $B-V$ | −0.0043 | +0.0360 | 0.016 | 31 |
| $I$..... | $V-I$ | +0.0405 | +0.0351 | 0.022 | 159 |

star candidates in three distinct regions of the CMD. The strongest signatures were at the level of the horizontal branch and represent candidate RR Lyrae stars. Weaker signatures were found at the RGB tip and just above the level of the MSTO. Several stars previously listed as variables were observed to be constant in our data set (see the appendix for details). We begin by discussing the variable HB stars.

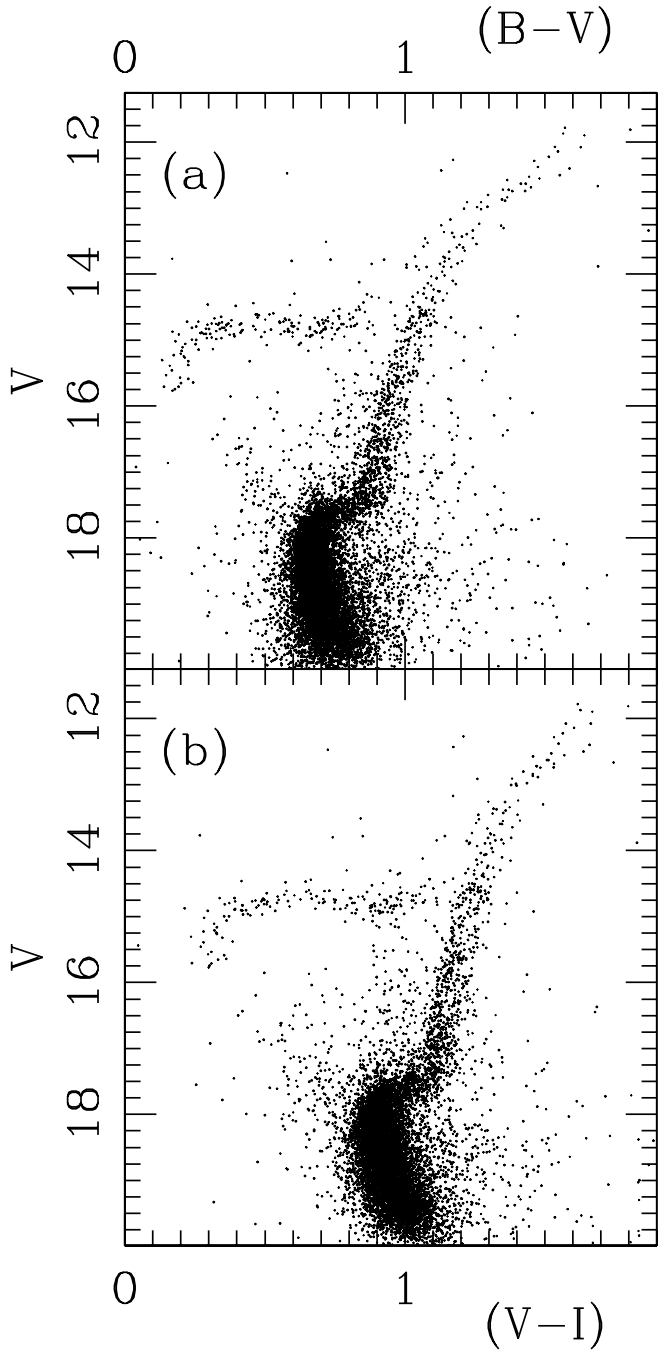


FIG. 2.—Color-magnitude diagrams of the stars in NGC 3201 listed in Table 2.

### 4.1. *RR Lyrae Stars*

In total, we detected 58 RR Lyrae star candidates in our data set. We cross-identified them with the list compiled by Clement et al. (2001) and found that all our candidates matched known RRLs.[2] Hereafter, we refer to the RRLs by their variable star designation (e.g., "V10") listed by Clement et al. (2001).

For each candidate RRL, we searched for a period in the range 0.2 days $< P <$ 0.9 days by using the template-fitting method of Layden & Sarajedini (2000) on the star's $V$-band data. Each of the 58 RRL candidates yielded a clear period and light curve. To complement this analysis, we also searched for periods in the range 0.2 days $< P <$ 2.0 days on the star's $B$-band data by using both the Lomb-Scargle method (Scargle 1982) and the string length method (K. von Braun & M. Mateo 2002, private communication). We also folded the light curve with the period listed in Cacciari (1984). In most cases, the periods from the different methods agreed well. In some cases, there were small but apparently real shifts from the Cacciari (1984) values, suggestive of the period changes described by Smith (1995).

The adopted period for each RRL is given in column (4) of Table 4. Column (2) of this table also lists the star's ID number from the left column of Table 2 and the star's Bailey type (ab = fundamental mode, c = first overtone; see col. [3]). The time series photometry for each RRL is presented in Table 5, where the columns include time of observation (HJD is the heliocentric Julian date minus 2,451,000 days), phase, magnitude and error, a code indicating the filter, the star's ID number from Table 2, and the variable star designation from Clement et al. (2001). Light curves of several representative RRLs are shown in Figure 3. A light curve for each of the 58 RRLs can be obtained electronically from the first author.[3]

Figure 4 shows the positions of the 58 RRLs in the CMD of NGC 3201. All 58 RRLs appear to be members of the cluster. We computed the light-curve parameters of each RRL from its observed data points. In Table 4, $E_{max}$ gives the epoch of maximum light in HJD defined above. Columns (6), (7), and (8), headed $\langle B\rangle$, $\langle V\rangle$, and $\langle I\rangle$, are the intensity-mean magnitudes in the respective filters. Columns (9), (10), and (11), headed $A_B$, $A_V$, and $A_I$, are the light-curve amplitudes in the respective filters. Column (12) of Table 4 lists comments associated with the period finding or light curves.

Preston (1959) defined the minimum light of an RRL to be the phases between 0.5 and 0.8 (Preston 1959). For each star, we calculated the arithmetic mean color (in magnitude units) of the points falling in this phase interval, along with the standard error of the mean. Columns (3) and (4) of Table 6 present, respectively, the mean $\langle B-V\rangle_{min}$ and standard error $\epsilon(B-V)$ computed from the $B-V$ colors, while columns (5) and (6) present the analogous values computed from the $V-I$ colors. Column (7) lists the number of data

[2] See the Appendix for details
[3] Visit http://physics.bgsu.edu/~layden/ASTRO/PUBL/published.html.

TABLE 4

PHOTOMETRY OF RR LYRAE VARIABLES

| Name (1) | ID (2) | Type (3) | Period (4) | $E_{max}$ (5) | $\langle B \rangle$ (6) | $\langle V \rangle$ (7) | $\langle I \rangle$ (8) | $A_B$ (9) | $A_V$ (10) | $A_I$ (11) | Comment (12) |
|---|---|---|---|---|---|---|---|---|---|---|---|
| V1 ..... | 269 | ab | 0.6048761 | 960.2698 | 15.42 | 14.81 | 13.97 | 1.18 | 0.92 | 0.62 | Blazhko? |
| V2 ..... | 179 | ab | 0.5326722 | 960.3673 | 15.35 | 14.80 | 14.01 | 1.37 | 1.07 | 0.73 | |
| V3 ..... | 284 | ab | 0.599410 | 960.5189 | 15.54 | 14.91 | 14.02 | 1.07 | 0.80 | 0.54 | |
| V4 ..... | 251 | ab | 0.6300096 | 960.3507 | 15.40 | 14.80 | 13.94 | 1.33 | 1.02 | 0.70 | |
| V5 ..... | 134 | ab | 0.501550 | 960.4593 | 15.23 | 14.73 | 14.04 | 1.19 | 0.94 | 0.61 | $0.2 < \phi < 0.75$ missing |
| V6 ..... | 256 | ab | 0.525260 | 960.4178 | 15.25 | 14.74 | 14.00 | 1.19 | 0.90 | 0.59 | Period uncertain |
| V7 ..... | 208 | ab | 0.6303322 | 960.3296 | 15.29 | 14.69 | 13.89 | 0.66 | 0.67 | 0.36 | |
| V8 ..... | 257 | ab | 0.6286573 | 960.5342 | 15.36 | 14.74 | 13.92 | 0.93 | 0.73 | 0.44 | Phases uncertain |
| V9 ..... | 309 | ab | 0.525530 | 960.5392 | 15.37 | 14.82 | 14.05 | 1.22 | 0.96 | 0.61 | |
| V10 ..... | 339 | ab | 0.5351644 | 961.4241 | 15.41 | 14.84 | 14.02 | 1.16 | 0.88 | 0.66 | No data at max |
| V11 ..... | 218 | c | 0.299049 | 961.4244 | 15.25 | 14.79 | 14.13 | 0.72 | 0.58 | 0.35 | |
| V12 ..... | 344 | ab | 0.4955547 | 961.0470 | 15.83 | 15.16 | 14.06 | 0.14 | 0.17 | 0.52 | No data at max |
| V13 ..... | 232 | ab | 0.5752145 | 961.0478 | 15.45 | 14.85 | 14.00 | 1.17 | 0.88 | 0.58 | |
| V14 ..... | 358 | ab | 0.5092945 | 961.3522 | 15.59 | 14.99 | 14.14 | 1.47 | 1.13 | 0.79 | |
| V15 ..... | 133 | ab | 0.5346644 | 951.3986 | 15.12 | 14.62 | 13.90 | 1.35 | 1.12 | 0.69 | |
| V16 ..... | 158 | c | 0.263438 | 960.4546 | 14.99 | 14.62 | 14.10 | 0.43 | 0.63 | 0.24 | |
| V17 ..... | 247 | ab | 0.565590 | 960.4595 | 15.32 | 14.76 | 13.96 | 1.18 | 0.92 | 0.63 | |
| V18 ..... | 258 | ab | 0.539655 | 960.5002 | 15.27 | 14.74 | 13.98 | 1.37 | 1.05 | 0.72 | |
| V19 ..... | 181 | ab | 0.525030 | 961.3556 | 15.28 | 14.73 | 13.98 | 1.10 | 0.92 | 0.67 | Few data points |
| V20 ..... | 120 | ab | 0.529100 | 961.2803 | 15.19 | 14.68 | 13.94 | 1.37 | 1.07 | 0.69 | Few data points |
| V21 ..... | 286 | ab | 0.566628 | 961.0939 | 15.42 | 14.83 | 14.01 | 0.95 | 0.73 | 0.56 | |
| V22 ..... | 260 | ab | 0.6059882 | 960.3204 | 15.34 | 14.75 | 13.93 | 1.10 | 0.86 | 0.58 | |
| V23 ..... | 283 | ab | 0.586775 | 960.1798 | 15.40 | 14.80 | 13.97 | 1.01 | 0.77 | 0.51 | |
| V24 ..... | 226 | ab | 0.5889534 | 961.5404 | 15.23 | 14.65 | 13.88 | 0.97 | 0.76 | 0.55 | |
| V25 ..... | 331 | ab | 0.514804 | 961.2822 | 15.24 | 14.73 | 14.00 | 1.38 | 1.05 | 0.71 | |
| V26 ..... | 304 | ab | 0.568968 | 960.5487 | 15.53 | 14.91 | 14.05 | 1.18 | 0.92 | 0.60 | |
| V27 ..... | 138 | ab | 0.484313 | 960.4818 | 15.25 | 14.76 | 14.03 | 1.49 | 1.21 | 0.79 | Few points at min |
| V28 ..... | 272 | ab | 0.580025 | 960.2400 | 15.48 | 14.87 | 14.02 | 1.09 | 0.86 | 0.55 | Scatter |
| V29 ..... | 244 | ab | 0.529120 | 961.2485 | 15.37 | 14.78 | 13.99 | 0.94 | 0.68 | 0.43 | Scatter, Blazhko? |
| V30 ..... | 233 | ab | 0.5158559 | 961.0870 | 15.10 | 14.60 | 13.93 | 1.17 | 0.87 | 0.68 | Few points at min |
| V31 ..... | 285 | ab | 0.519120 | 961.1771 | 15.49 | 14.90 | 14.07 | 1.62 | 1.26 | 0.80 | Scatter at min |
| V32 ..... | 175 | ab | 0.5611656 | 961.5623 | 15.26 | 14.73 | 13.98 | 1.60 | 1.24 | 0.80 | |
| V35 ..... | 288 | ab | 0.6155244 | 961.3318 | 15.35 | 14.75 | 13.93 | 0.81 | 0.63 | 0.42 | |
| V36 ..... | 165 | ab | 0.484178 | 960.4155 | 15.21 | 14.73 | 14.02 | 1.55 | 1.26 | 0.85 | Min poorly defined |
| V37 ..... | 240 | ab | 0.575740 | 960.3581 | 15.31 | 14.74 | 13.95 | 1.03 | 1.05 | 0.46 | Scatter, Blazhko? |
| V38 ..... | 329 | ab | 0.509090 | 960.5026 | 15.34 | 14.81 | 14.05 | 1.03 | 0.81 | 0.66 | Blazhko? |
| V39 ..... | 330 | ab | 0.483233 | 960.5890 | 15.32 | 14.81 | 14.08 | 1.51 | 1.20 | 0.80 | |
| V40 ..... | 300 | ab | 0.643820 | 960.1597 | 15.46 | 14.84 | 13.95 | 0.56 | 0.58 | 0.29 | |
| V42 ..... | 171 | ab | 0.5382490 | 961.3917 | 15.11 | 14.61 | 13.89 | 1.35 | 1.22 | 0.68 | |
| V44 ..... | 186 | ab | 0.6107344 | 960.5237 | 15.37 | 14.76 | 13.92 | 0.81 | 0.62 | 0.44 | |
| V45 ..... | 278 | ab | 0.537460 | 960.1787 | 15.49 | 14.91 | 14.09 | 1.45 | 1.09 | 0.73 | Blazhko |
| V47 ..... | 160 | ab | 0.521210 | 961.5714 | 15.15 | 14.65 | 13.94 | 1.19 | 0.89 | 0.57 | |
| V48 ..... | 161 | c | 0.341272 | 953.5484 | 15.17 | 14.68 | 14.02 | 0.56 | 0.65 | 0.28 | |
| V49 ..... | 274 | ab | 0.581020 | 961.1356 | 15.27 | 14.72 | 13.95 | 1.36 | 1.04 | 0.69 | |
| V50 ..... | 188 | ab | 0.542178 | 960.3527 | 15.25 | 14.71 | 13.93 | 1.31 | 1.00 | 0.68 | |
| V51 ..... | 199 | ab | 0.518600 | 960.3791 | 15.23 | 14.72 | 14.02 | 1.50 | 1.16 | 0.78 | Scatter, Blazhko? |
| V71 ..... | 167 | ab | 0.601190 | 960.2549 | 15.25 | 14.70 | 13.90 | 1.02 | 0.78 | 0.50 | |
| V73 ..... | 211 | ab | 0.519965 | 961.2613 | 15.27 | 14.76 | 14.01 | 1.65 | 1.24 | 0.82 | |
| V76 ..... | 287 | ab | 0.526680 | 960.4026 | 15.37 | 14.81 | 14.01 | 0.84 | 0.66 | 0.78 | Blazhko? |
| V77 ..... | 243 | ab | 0.567644 | 960.1222 | 15.27 | 14.71 | 13.93 | 1.17 | 0.86 | 0.59 | |
| V78 ..... | 213 | ab | 0.513900 | 960.5244 | 15.38 | 14.85 | 14.05 | 1.29 | 1.00 | 0.66 | |
| V80 ..... | 301 | ab | 0.589960 | 960.4004 | 15.38 | 14.80 | 13.97 | 0.75 | 0.59 | 0.41 | |
| V81 ..... | 297 | ab | 0.519753 | 960.3730 | 15.37 | 14.83 | 14.04 | 1.42 | 1.13 | 0.74 | |
| V83 ..... | 281 | ab | 0.5451998 | 961.3221 | 15.33 | 14.78 | 14.01 | 1.58 | 1.23 | 0.82 | |
| V90 ..... | 173 | ab | 0.606105 | 960.0304 | 15.24 | 14.68 | 13.89 | 1.21 | 0.94 | 0.60 | |
| V92 ..... | 212 | ab | 0.539585 | 960.3016 | 15.31 | 14.76 | 13.98 | 1.29 | 0.99 | 0.69 | |
| V98 ..... | 150 | c | 0.335647 | 960.4483 | 15.21 | 14.78 | 14.09 | 0.55 | 0.43 | 0.27 | Lee 1405 |
| V100 ..... | 223 | ab | 0.548920 | 960.1415 | 15.32 | 14.77 | 13.99 | 1.28 | 1.02 | 0.71 | Lee 2710 |

TABLE 5

TIME SERIES PHOTOMETRY OF VARIABLE STARS

| HJD | $\phi$ | Mag | $\sigma_m$ | Band[a] | ID | Name |
|---|---|---|---|---|---|---|
| 212.62287..... | 0.967 | 14.979 | 0.004 | 41 | 269 | V1 |
| 212.62439..... | 0.969 | 14.437 | 0.005 | 93 | 269 | V1 |
| 212.62558..... | 0.971 | 13.737 | 0.007 | 30 | 269 | V1 |
| 212.68878..... | 0.076 | 14.806 | 0.003 | 41 | 269 | V1 |
| 212.69042..... | 0.078 | 14.351 | 0.005 | 93 | 269 | V1 |
| 212.69168..... | 0.080 | 13.681 | 0.009 | 30 | 269 | V1 |

NOTE.—Table 5 is presented in its entirety in the electronic edition of the Astronomical Journal. A portion is shown here for guidance regarding its form and content.

[a] Filter through which the photometry was taken, according to the following code: $V = 93$, $B = 41$, and $I = 30$ (1999 season) or 81 (2001 season).

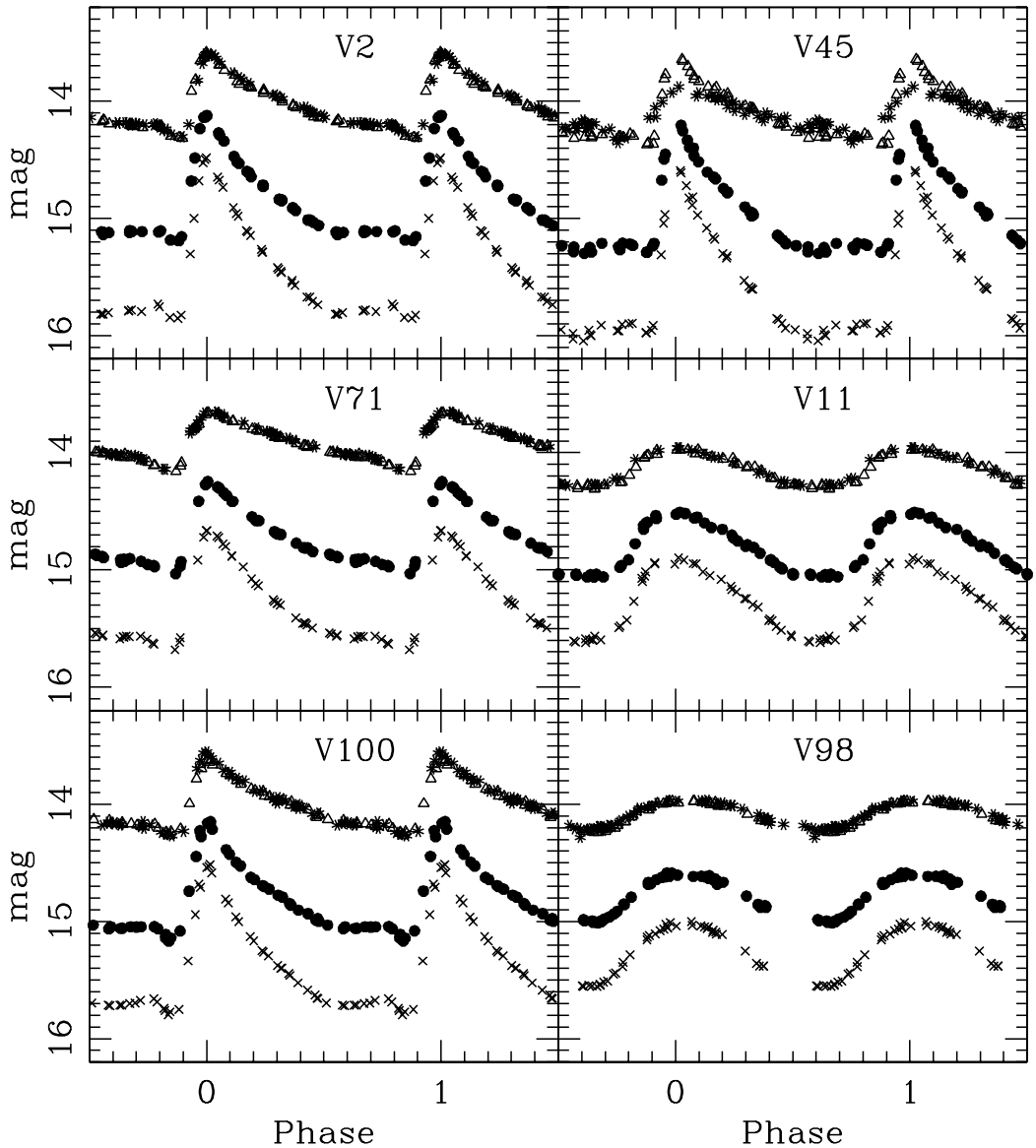


FIG. 3.—Light curves for six of the 58 RRLs observed in NGC 3201, showing *B* magnitudes (*crosses*), *V* magnitudes (*circles*), *I* magnitudes for the 1999 data (*triangles*), and *I* magnitudes for the 2001 data (*asterisks*). *Left*, Three curves for typical RRab (fundamental mode) stars; *right top*, RRab star that exhibits the Blazhko effect; *right middle and bottom*, typical RRc (first overtone) stars. Each star is labeled with its name from Table 4.

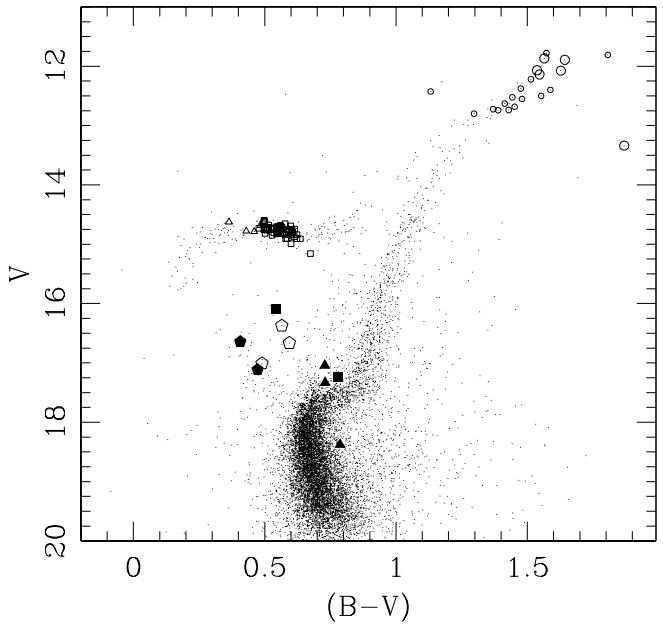


FIG. 4.—Locations of the variable stars in the ($V$, $B-V$) CMD from Fig. 2, showing RR Lyrae stars: Rab's (*open squares*) and RRc's (*open triangles*), variable red giant stars (*circles*; larger circles mark stars with amplitudes $A_V \geq 0.03$ mag), $\delta$ Scuti stars (*pentagons*; filled pentagons indicate probable, open pentagons indicate possible), detached binaries (EA type; *filled squares*), and contact binaries (W UMa type; *filled triangles*).

points in the minimum-light phase interval. We will use these data in § 5 to determine the interstellar reddening toward NGC 3201.

### 4.2. *RGB Variables*

We found that stars within about 1 mag of the RGB tip had elevated values of $\Lambda$, the DAOPHOT variability index (Fig. 5*a*). None of these stars were near digital CCD saturation in the 1999 images,[4] so the effect is real. Figure 6 confirms this: the *BVI* magnitudes vary slowly and smoothly as a function of time, and the variations are correlated in the different passbands. From the distribution of points in Figure 5*a*, we chose to search closely for variability in stars with $\Lambda > 2.5$. We included all stars with $V < 12.8$ to provide unbiased statistics on stars nearest the RGB tip. Figure 7 shows the $V$-band light curves for the RGB variable star candidates in NGC 3201.

Figure 4 shows the location of the RGB variables in the CMD. With the exception of two or three field stars, most appear to be members of NGC 3201.

Since many of the stars complete at least one light cycle, we can estimate the photometric amplitudes of the stars. To minimize the effects of photometric scatter on the low-amplitude RGB variables, we defined a star's amplitude as the magnitude difference between the third-brightest and third-faintest observations in each passband. Table 7 lists the amplitudes in each passband ($A_V$, $A_B$, and $A_I$) of the variable candidates, along with their identification number from Table 2, their mean $V$ magnitude, and their variability index, $\Lambda$. Figure 5*b* shows the $V$ amplitude as a function of

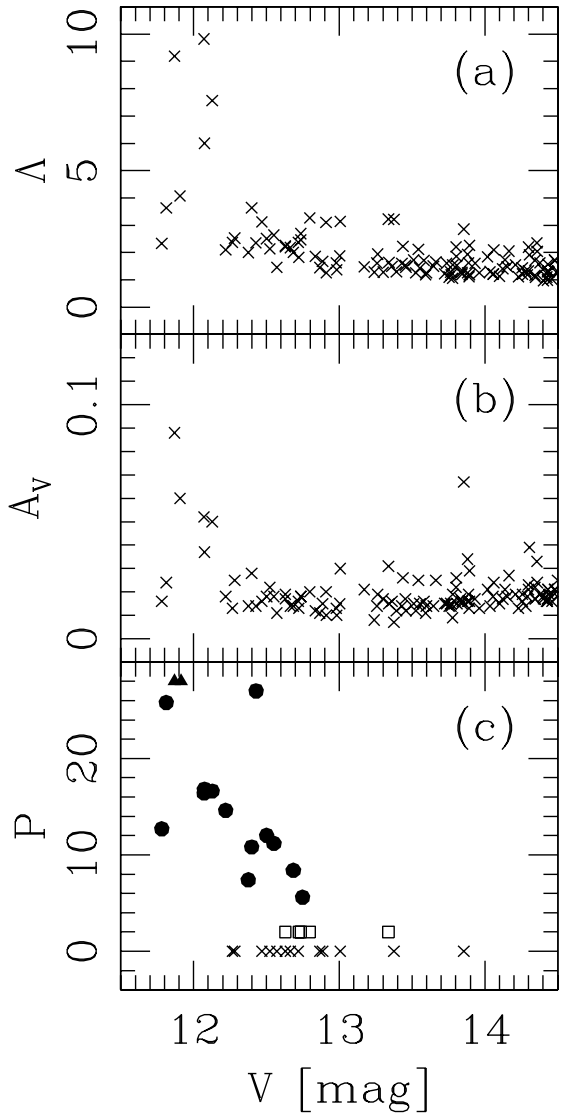


FIG. 5.—Properties of the variable RGB stars in NGC 3201. (*a*) DAOPHOT variability index (Stetson 1994) plotted as a function of $V$ magnitude. Stars with $\Lambda > 2.5$ and $V < 12.8$ were targeted for more intensive study. (*b*) $V$-band photometric amplitude (see § 4.2) plotted against $V$ magnitude. (*c*) Estimated periods, in days, for stars identified in (*a*). Circles indicate stars that were well-fitted with a sinusoid. Triangles indicate stars with periods longer than 30 days. Squares indicate stars with apparently irregular variations ($P = 2$ assumed for display purposes). Crosses indicate stars with no significant photometric variation.

$V$ magnitude for these stars (the point with $A_V \approx 0.7$ and $V \approx 13.8$ is a spurious artifact of poor photometry at the image edge). The amplitudes tend to be largest near the RGB tip, suggesting these stars may be just reaching the temperatures at which pulsation instabilities arise in irregular, semiregular, and Mira type variables. However, the amplitudes in the NGC 3201 stars are quite small, suggesting they are better associated with the small-amplitude red variables (SARVs) defined by Eggen (1977). Recent study has shown that most SARVs pulsate in one or more low-order radial modes (Percy, Wilson, & Henry 2001).

Though the temporal coverage of our RGB variables is short, in some cases their variations appear roughly sinusoidal. We have fitted the light curves of these stars with sine curves by using the template-fitting method discussed in

[4] The brightest RGB stars *were* saturated in the 2001 $I$-band images; we do not include those data in this analysis.

TABLE 6

COLOR AND REDDENING OF RR LYRAE VARIABLES

| Name (1) | Type (2) | $\langle B-V\rangle_{\rm min}$ (3) | $\epsilon(B-V)$ (4) | $\langle V-I\rangle_{\rm min}$ (5) | $\epsilon(V-I)$ (6) | $N_{\rm min}$ (7) | $E(B-V)$ (8) | $E(V-I)$ (9) |
|---|---|---|---|---|---|---|---|---|
| V1 ..... | ab | 0.702 | 0.004 | 0.940 | 0.009 | 13 | 0.297 | 0.370 |
| V2 ..... | ab | 0.675 | 0.008 | 0.924 | 0.010 | 9 | 0.283 | 0.354 |
| V3 ..... | ab | 0.725 | 0.004 | 0.963 | 0.006 | 12 | 0.321 | 0.393 |
| V4 ..... | ab | 0.722 | 0.003 | 0.959 | 0.006 | 13 | 0.312 | 0.389 |
| V5[a] ..... | ab | 0.609 | 0.003 | 0.829 | 0.005 | 3 | 0.223 | 0.259 |
| V6[a] ..... | ab | 0.633 | 0.005 | 0.894 | 0.022 | 13 | 0.243 | 0.324 |
| V7 ..... | ab | 0.637 | 0.005 | 0.878 | 0.018 | 12 | 0.227 | 0.308 |
| V8[a] ..... | ab | 0.667 | 0.015 | 0.915 | 0.012 | 20 | 0.257 | 0.345 |
| V9 ..... | ab | 0.658 | 0.003 | 0.941 | 0.026 | 24 | 0.268 | 0.371 |
| V10 ..... | ab | 0.684 | 0.013 | 1.000 | 0.039 | 13 | 0.292 | 0.430 |
| V11 ..... | c | 0.533 | 0.006 | 0.824 | 0.038 | 14 | ... | ... |
| V12 ..... | ab | 0.670 | 0.004 | 0.884 | 0.006 | 21 | 0.285 | 0.314 |
| V13 ..... | ab | 0.673 | 0.034 | 0.986 | 0.031 | 13 | 0.273 | 0.416 |
| V14 ..... | ab | 0.760 | 0.023 | 1.022 | 0.053 | 16 | 0.373 | 0.452 |
| V15 ..... | ab | 0.621 | 0.010 | 0.893 | 0.034 | 11 | 0.229 | 0.323 |
| V16 ..... | c | 0.379 | 0.022 | 0.638 | 0.034 | 13 | ... | ... |
| V17 ..... | ab | 0.656 | 0.003 | 0.900 | 0.007 | 15 | 0.258 | 0.330 |
| V18 ..... | ab | 0.656 | 0.006 | 0.888 | 0.006 | 10 | 0.263 | 0.318 |
| V19[a] ..... | ab | 0.637 | 0.010 | 0.888 | 0.010 | 3 | 0.247 | 0.318 |
| V20[a] ..... | ab | 0.645 | 0.020 | 0.878 | 0.019 | 3 | 0.254 | 0.308 |
| V21 ..... | ab | 0.674 | 0.004 | 0.900 | 0.009 | 11 | 0.276 | 0.330 |
| V22 ..... | ab | 0.662 | 0.005 | 0.925 | 0.014 | 12 | 0.257 | 0.355 |
| V23 ..... | ab | 0.678 | 0.003 | 0.929 | 0.011 | 25 | 0.276 | 0.359 |
| V24 ..... | ab | 0.586 | 0.049 | 0.973 | 0.035 | 14 | 0.184 | 0.403 |
| V25 ..... | ab | 0.642 | 0.006 | 0.874 | 0.007 | 13 | 0.254 | 0.304 |
| V26 ..... | ab | 0.720 | 0.003 | 0.962 | 0.010 | 10 | 0.321 | 0.392 |
| V27[a] ..... | ab | 0.675 | 0.018 | 0.870 | 0.015 | 3 | 0.292 | 0.300 |
| V28 ..... | ab | 0.687 | 0.004 | 0.941 | 0.005 | 14 | 0.286 | 0.371 |
| V29 ..... | ab | 0.643 | 0.007 | 0.891 | 0.024 | 10 | 0.252 | 0.321 |
| V30[a] ..... | ab | 0.613 | 0.010 | 0.857 | 0.020 | 8 | 0.224 | 0.287 |
| V31[a] ..... | ab | 0.740 | 0.007 | 0.987 | 0.011 | 11 | 0.351 | 0.417 |
| V32 ..... | ab | 0.672 | 0.007 | 0.918 | 0.007 | 10 | 0.275 | 0.348 |
| V35 ..... | ab | 0.668 | 0.003 | 0.898 | 0.004 | 15 | 0.261 | 0.328 |
| V36[a] ..... | ab | 0.615 | 0.007 | 0.974 | 0.085 | 10 | 0.232 | 0.404 |
| V37 ..... | ab | 0.595 | 0.044 | 0.913 | 0.018 | 20 | 0.195 | 0.343 |
| V38 ..... | ab | 0.610 | 0.011 | 0.853 | 0.011 | 31 | 0.223 | 0.283 |
| V39 ..... | ab | 0.644 | 0.004 | 0.883 | 0.006 | 17 | 0.261 | 0.313 |
| V40 ..... | ab | 0.655 | 0.043 | 0.984 | 0.032 | 13 | 0.243 | 0.414 |
| V42 ..... | ab | 0.592 | 0.029 | 0.938 | 0.052 | 14 | 0.199 | 0.368 |
| V44 ..... | ab | 0.676 | 0.004 | 0.914 | 0.004 | 13 | 0.270 | 0.344 |
| V45[a] ..... | ab | 0.716 | 0.006 | 0.964 | 0.009 | 11 | 0.323 | 0.394 |
| V47 ..... | ab | 0.596 | 0.007 | 0.841 | 0.007 | 12 | 0.206 | 0.271 |
| V48 ..... | c | 0.535 | 0.003 | 0.783 | 0.025 | 11 | ... | ... |
| V49 ..... | ab | 0.675 | 0.004 | 0.904 | 0.007 | 18 | 0.274 | 0.334 |
| V50 ..... | ab | 0.658 | 0.005 | 0.896 | 0.008 | 12 | 0.264 | 0.326 |
| V51[a] ..... | ab | 0.635 | 0.011 | 0.842 | 0.009 | 11 | 0.246 | 0.272 |
| V71 ..... | ab | 0.659 | 0.004 | 0.925 | 0.029 | 13 | 0.255 | 0.355 |
| V73 ..... | ab | 0.670 | 0.004 | 0.905 | 0.007 | 12 | 0.281 | 0.335 |
| V76 ..... | ab | 0.641 | 0.005 | 0.877 | 0.014 | 20 | 0.250 | 0.307 |
| V77 ..... | ab | 0.660 | 0.005 | 0.868 | 0.006 | 12 | 0.262 | 0.298 |
| V78 ..... | ab | 0.653 | 0.003 | 0.894 | 0.009 | 15 | 0.265 | 0.324 |
| V80 ..... | ab | 0.646 | 0.004 | 0.886 | 0.006 | 14 | 0.244 | 0.316 |
| V81 ..... | ab | 0.673 | 0.006 | 0.918 | 0.006 | 13 | 0.284 | 0.348 |
| V83 ..... | ab | 0.684 | 0.005 | 0.933 | 0.006 | 16 | 0.290 | 0.363 |
| V90 ..... | ab | 0.661 | 0.003 | 0.897 | 0.004 | 13 | 0.256 | 0.327 |
| V92 ..... | ab | 0.674 | 0.019 | 0.928 | 0.048 | 14 | 0.281 | 0.358 |
| V98 ..... | c | 0.506 | 0.032 | 0.766 | 0.014 | 14 | ... | ... |
| V100 ..... | ab | 0.647 | 0.006 | 0.884 | 0.007 | 10 | 0.252 | 0.314 |

[a] See the relevant comment in Table 4.

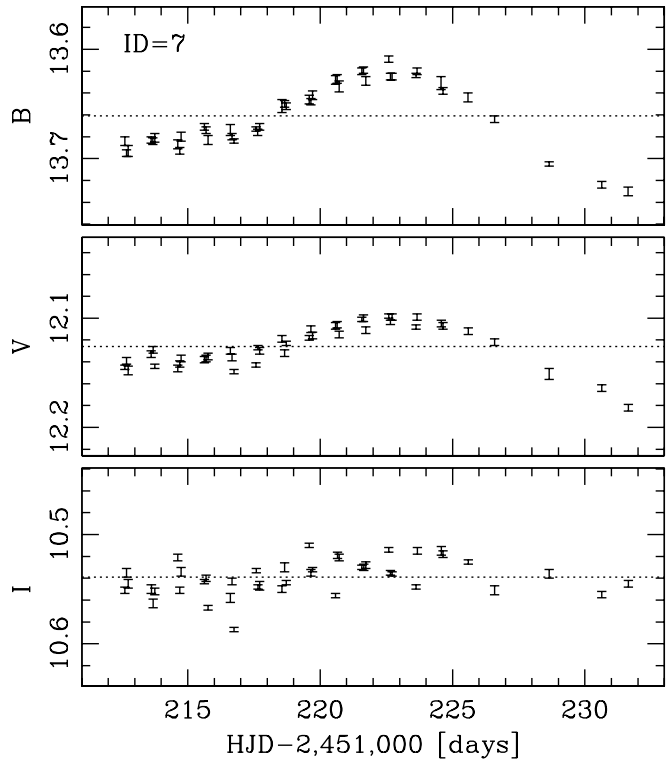


FIG. 6.—*B*, *V*, and *I* magnitudes of the RGB star 7 plotted against time. Dotted lines mark the mean magnitudes of the variable.

§ 4.1. The resulting periods are listed in Table 7 under the heading "Per." Until these stars are observed over much longer intervals of time, these values should be considered "characteristic variation timescales" rather than formal periods. With the exception of star 32, no attempt was made to fit stars with $V > 13$ since their amplitudes are so small. Figure 5*c* shows the periods plotted against $V$ magnitude. There is a trend for more luminous stars to have longer periods. The stars with irregular light curves may represent transition objects between nonvariable and regularly pulsating stars.

The amplitudes and periods presented herein are estimates based on our relatively small range of observing epochs. Monitoring over timescales of months or years is needed to establish these values firmly. The study of SARVs in globular clusters may help clarify the onset of pulsational instability in red giant and asymptotic giant branch stars, since a globular cluster presents a spectrum of temperatures and surface gravities at a fixed age, metallicity, and distance modulus. Large-format, queue-scheduled CCD detectors can efficiently continue the research on SARVs in globular clusters begun by Eggen (1977 and references therein).

### 4.3. *Variables below the HB*

A few stars fainter than the HB showed elevated levels of the variability index, $\Lambda$. We selected for study all the stars with $\Lambda$ 3 or more times larger than the median $\Lambda$ at that magnitude. Photometric amplitudes for each star were measured as described in the previous section. Table 8 gives the

TABLE 7
PHOTOMETRY OF RGB VARIABLES

| ID | $\bar{V}$ | $\Lambda$ | $A_V$ | $A_B$ | $A_I$ | Per | Comment |
|---|---|---|---|---|---|---|---|
| 1..... | 11.778 | 2.33 | 0.016 | 0.032 | 0.025 | 13 | |
| 2..... | 11.809 | 3.63 | 0.024 | 0.038 | 0.029 | 26 | Field? |
| 3..... | 11.868 | 9.19 | 0.088 | 0.151 | 0.085 | >30 | V79, incomplete |
| 4..... | 11.892 | 6.79 | 0.044 | 0.076 | 0.044 | >30 | Incomplete |
| 5..... | 12.069 | 9.82 | 0.052 | 0.067 | 0.041 | 16 | |
| 6..... | 12.075 | 6.00 | 0.037 | 0.055 | 0.041 | 17 | |
| 7..... | 12.138 | 7.56 | 0.050 | 0.075 | 0.043 | 17 | Irr? |
| 8..... | 12.220 | 2.10 | 0.018 | 0.017 | 0.036 | 15 | |
| 9..... | 12.263 | 2.37 | 0.013 | 0.034 | 0.041 | ... | Nonvar |
| 10..... | 12.282 | 2.53 | 0.025 | 0.039 | 0.051 | ... | Nonvar |
| 11..... | 12.376 | 2.00 | 0.014 | 0.022 | 0.041 | 7 | |
| 12..... | 12.399 | 3.64 | 0.028 | 0.036 | 0.038 | 11 | |
| 13..... | 12.426 | 2.35 | 0.014 | 0.012 | 0.028 | 27 | Nonvar? Field? |
| 14..... | 12.470 | 3.12 | 0.016 | 0.037 | 0.025 | ... | Few points |
| 15..... | 12.501 | 2.51 | 0.018 | 0.030 | 0.037 | 12 | |
| 16..... | 12.523 | 2.14 | 0.022 | 0.025 | 0.038 | ... | Irr |
| 17..... | 12.551 | 2.64 | 0.018 | 0.030 | 0.041 | 11 | |
| 18..... | 12.572 | 1.46 | 0.011 | 0.011 | 0.044 | ... | Nonvar |
| 19..... | 12.629 | 2.21 | 0.019 | 0.023 | 0.037 | ... | Irr |
| 20..... | 12.630 | 2.25 | 0.017 | 0.031 | 0.042 | ... | Nonvar |
| 21..... | 12.661 | 2.18 | 0.014 | 0.035 | 0.034 | ... | Nonvar |
| 22..... | 12.682 | 2.00 | 0.014 | 0.022 | 0.031 | 8 | |
| 23..... | 12.718 | 2.37 | 0.016 | 0.024 | 0.043 | ... | Nonvar |
| 24..... | 12.722 | 1.82 | 0.013 | 0.014 | 0.042 | ... | Irr? |
| 25..... | 12.737 | 2.46 | 0.018 | 0.019 | 0.036 | ... | Irr? |
| 26..... | 12.741 | 2.10 | 0.017 | 0.028 | 0.021 | 6 | |
| 27..... | 12.799 | 3.27 | 0.020 | 0.028 | 0.041 | ... | Irr? |
| 29..... | 12.863 | 1.45 | 0.011 | 0.017 | 0.018 | ... | Nonvar |
| 30..... | 12.882 | 1.68 | 0.015 | 0.016 | 0.028 | ... | Nonvar |
| 36..... | 13.006 | 3.14 | 0.030 | 0.048 | 0.057 | ... | Nonvar |
| 32..... | 13.338 | 3.22 | 0.031 | 0.037 | 0.036 | ... | Field, Irr? |

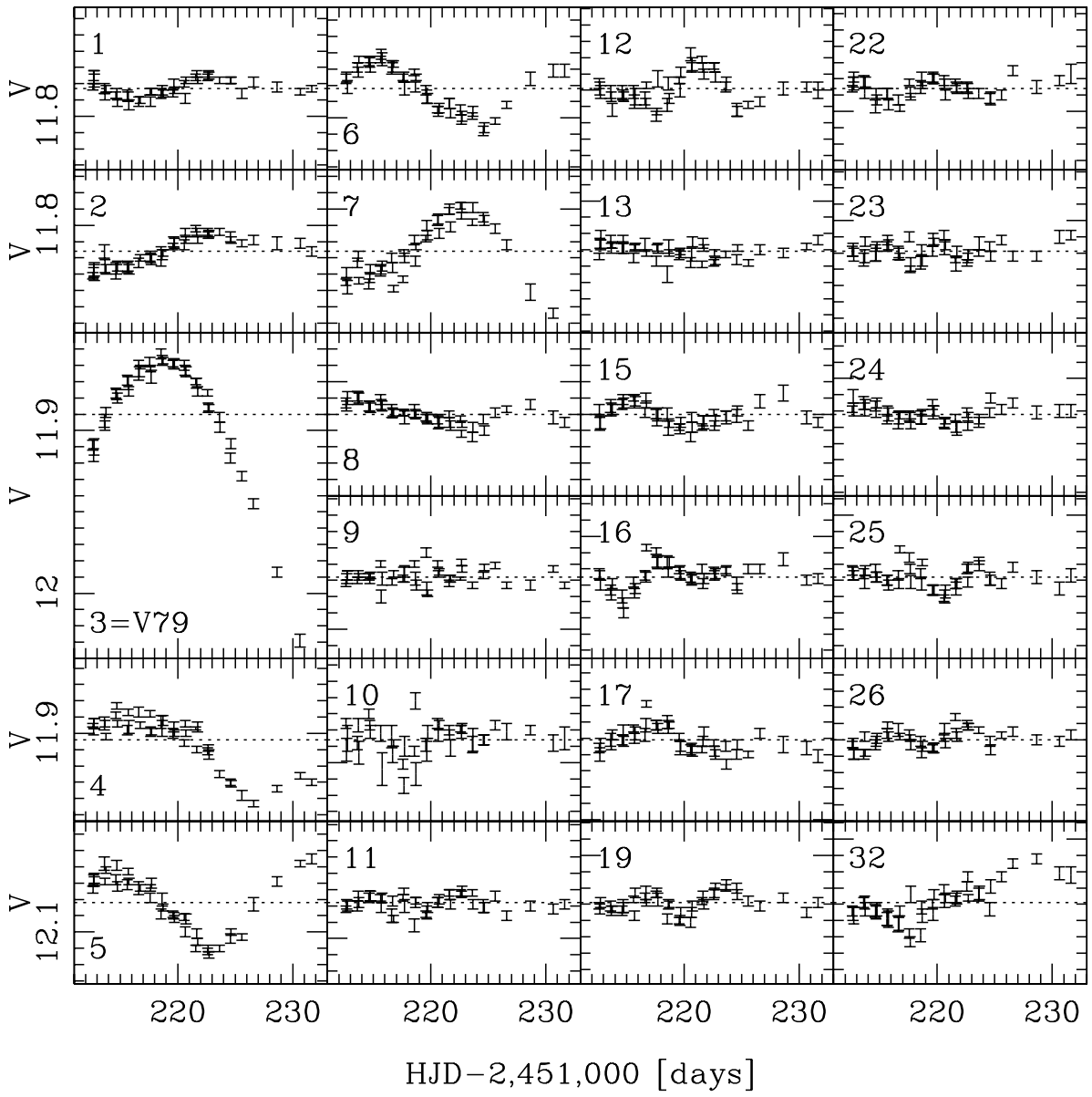


FIG. 7.—$V$ magnitudes of the variable RGB stars plotted against time. Dotted lines mark the mean magnitudes of the variable. The scale is the same for each plot: minor ticks are 0.01 mag. The nonvariable stars 9, 10, and 23 are included for comparison.

TABLE 8
PHOTOMETRY OF SUB-HB VARIABLES

| ID | $\bar{V}$ | $\Lambda$ | $A_V$ | $A_B$ | $A_I$ | Period | Type | Comment |
|---|---|---|---|---|---|---|---|---|
| 967 | 17.045 | 8.45 | 0.401 | 0.411 | 0.345 | 0.44179 | W UMa | vBM No. 4 (their period) |
| 752 | 16.642 | 8.36 | 0.308 | 0.374 | 0.208 | 0.05019 | $\delta$ Scuti | |
| 776 | 16.665 | 7.04 | 0.530 | 0.608 | 0.444 | 0.08807 | $\delta$ Scuti? | Crowded |
| 1218 | 17.332 | 5.52 | 0.361 | 0.373 | 0.337 | 0.377114 | W UMa | vBM No. 3 (their period) |
| 651 | 16.373 | 5.31 | 0.274 | 0.392 | 0.144 | 0.06303 | $\delta$ Scuti? | $P = 0.06734$ possible |
| 564 | 16.094 | 5.28 | 0.273 | 0.354 | 0.246 | 5.84 | EA? | Blended image |
| 1019 | 17.113 | 4.19 | 0.296 | 0.359 | 0.187 | 0.05428 | $\delta$ Scuti | $P = 0.05742$ possible |
| 1120 | 17.227 | 4.13 | 0.421 | 0.487 | 0.125 | 2.84810 | EA | vBM No. 12 (their period) |
| 941 | 17.010 | 2.82 | 0.207 | 0.215 | 0.217 | 0.03735 | $\delta$ Scuti? | Crowded |
| 4396 | 18.375 | 1.80 | 0.245 | 0.259 | 0.336 | 0.345095 | W UMa | vBM No. 2 (their period) |

ID number matching those in Table 2, the mean $V$ magnitude, and the variability index $\Lambda$ for each candidate.

We then used the template-fitting technique (§ 4.1) to search for the period of each star. In most cases, one template (light-curve shape) and period provided a fit significantly better than any other. The period and variability type listed in Table 8 reflect this fit. Three of the stars, Nos. 967, 1120, and 1218, were discovered by von Braun & Mateo (2002). We include in Table 8 another faint variable discovered by von Braun & Mateo (2002) that is in our field, but whose variability was below our signal-to-noise threshold (vBM No. 2). These stars consisted of three W Ursae Majoris type contact binaries and a detached binary (EA type). One additional faint variable star candidate, No. 564, appears to be a detached binary, though the four magnitude drops shown in Figure 8 could be a result of crowding-induced photometric errors.

Among our newly discovered faint variables are two stars that are clearly $\delta$ Scuti pulsating variables (Nos. 752 and 1019). Their light curves are shown in Figure 8. We list three other variables as possible $\delta$ Scuti stars (DSSs), but larger scatter in their light curves leaves the interpretation uncertain. The scatter may be observational (due to photometric crowing effects) or it may be real (a result of more than one period being excited in the star). Intensive observation of these three stars is required to clarify their nature. The possible DSS with the largest light-curve scatter, Nos. 651, is blended in our images with a known RRL, V36. Our photometric procedure may have accidentally attributed some of the light from V36 to No. 651. It is therefore likely that star 651 is not actually variable at all.

Figure 4 shows that the probable DSSs, along with No. 941, inhabit the blue straggler region of NGC 3201, precisely where most globular cluster DSSs are found. This increases the likelihood that they are DSSs and that they are members of NGC 3201. Stars 651 and 776 are significantly brighter and redder than the blue straggler sequence in NGC 3201. This and its longer period suggest that star 776 is a foreground DSS with [Fe/H] $\gtrsim -1.0$ dex (McNamara 1997). The $\delta$ Scuti stars will be discussed at length in § 6.2.

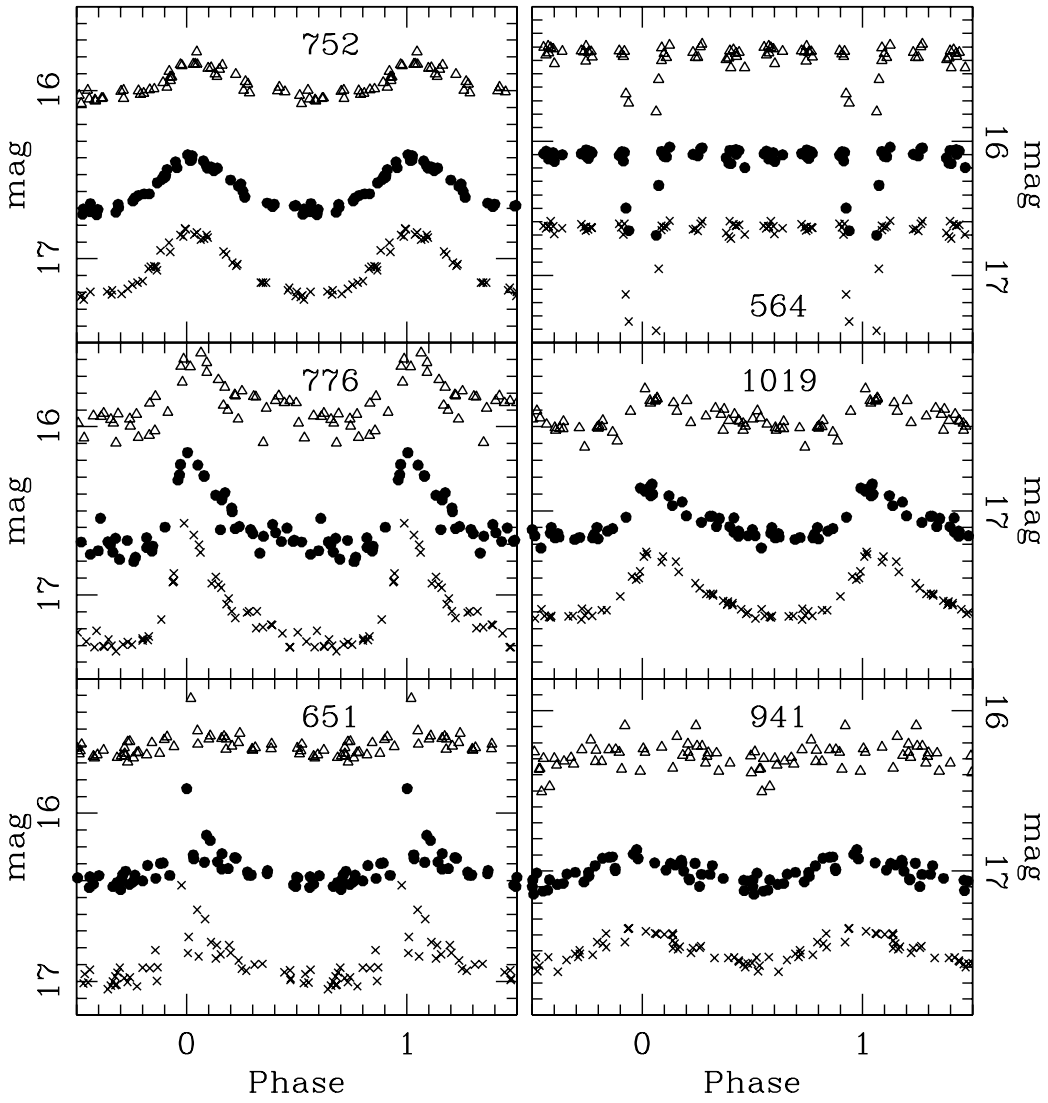


FIG. 8.—Light curves for the six new variables discovered below the magnitude of the HB. Symbols indicate $B$ (*crosses*), $V$ (*circles*), and $I$ (*triangles*) magnitudes. Two cycles are shown for continuity. Each star is labeled with its identification (ID) number from Tables 2 and 8.

## 5. REDDENING

Before discussing the interstellar reddening of NGC 3201, we must establish the relations between reddening and extinction in the filter passbands used in this study. We computed the effective wavelengths of the *BVI* filters used at the YALO telescope and by using the relations of Cardelli, Clayton, & Mathis (1989) obtained $A(B)/E(B-V) = 4.045$, $A(V)/E(B-V) = 3.045$, $A(I)/E(B-V) = 1.833$, and $E(V-I)/E(B-V) = 1.212$.

Sturch (1966) and Blanco (1992) demonstrated how the reddening of an ab type RRL can be determined from its observed minimum-light color. Equation (7) of Blanco (1992) relates the $E(B-V)$ for a given star to the star's apparent $B-V$ color at minimum light, its pulsation period, and its metallicity (expressed as $\Delta S$). For NGC 3201, we adopted [Fe/H] $= -1.53$ from the extensive compilation of Rutledge, Hesser, & Stetson (1997), and converted this value (which is on the system of Zinn & West 1984) to $\Delta S$ using equation (6) of Layden (1994). The $E(B-V)$ values computed for each RRL, assuming $\Delta S = 6.9$, are listed in column (8) of Table 6. Rutledge et al. (1997) estimated the external uncertainty in their [Fe/H] values to be $\sim$0.2 dex, corresponding to 1.4 units in $\Delta S$. If the [Fe/H] of NGC 3201 is 0.2 dex more metal-rich than our assumed metallicity, the $E(B-V)$ values in Table 6 become 0.01 mag smaller.

For each star, we computed $E(V-I)$ from the minimum-light $V-I$ color in Table 6 and the intrinsic minimum-light color, $\langle V-I\rangle_{\rm min,0} = 0.57$, from Day et al. (2002). The resulting $E(V-I)$ value for each star is listed in column (9) of Table 6. The Day et al. (2002) calibration is based on only 15 points, so it is less secure than the $B-V$ relation. There is also some ambiguity in the dependence of $\langle V-I\rangle_{\rm min,0}$ with metallicity: $\langle V-I\rangle_{\rm min,0}$ is largest at [Fe/H] $= -1.6$ and falls off slightly for more metal-rich and metal-poor stars. If we consider only the nine stars with $-2 <$ [Fe/H] $< -1$, we find $\langle V-I\rangle_{\rm min,0} = 0.58$ with an rms scatter of 0.023 mag. The derived $E(V-I)$ values in Table 6 would then be systematically smaller by 0.01 mag.

The mean reddenings based on the 54 RRab stars in Table 6 are $\langle E(B-V)\rangle = 0.264 \pm 0.005$ mag (rms $= 0.036$ mag) and $\langle E(V-I)\rangle = 0.343 \pm 0.006$ mag (rms $= 0.043$ mag). The $E(B-V)$ values range from 0.18 to 0.37 mag, and the $E(V-I)$ values range from 0.26 to 0.45 mag, confirming the spatial variability of the reddening in this field discussed by von Braun & Mateo (2001) and others listed therein. Given this variation, it is best to quote mean reddenings for a small, well-defined region near the cluster center where the concentration of stars is highest. For the 21 RRab's within 2.′0 of the cluster center, we find $\langle E(B-V)\rangle = 0.252 \pm 0.004$ mag (rms $= 0.021$ mag) and $\langle E(V-I)\rangle = 0.335 \pm 0.008$ mag (rms $= 0.037$ mag). The uncertainty in our photometric zero point (see Table 3) places a systematic uncertainty of $\sim$0.02 mag on our mean reddening estimates.

Piersimoni et al. (2002) obtained *BVI* CCD light curves for many of the RRab's studied herein. Instead of using minimum-light colors, they developed a series of reddening relations based on colors averaged over the entire RRL light curve. For NGC 3201, they obtained $\langle E(B-V)\rangle = 0.30 \pm 0.03$ mag and $\langle E(V-I)\rangle = 0.36 \pm 0.05$ mag. Our reddening estimates are slightly lower than those of Piersimoni et al. (2002). Their photometry was calibrated directly to that of Stetson (2000), and Table 1 shows that our photometry is $\sim$0.05 mag bluer in $B-V$ than that of Stetson (2000). Thus, the reddening difference in $B-V$ can be completely accounted for by this difference. Similarly, our photometry is $\sim$0.01 mag redder in $V-I$ than that of Stetson (2000).

A number of previous authors have estimated the reddening of NGC 3201. Cacciari (1984) derived $E(B-V) = 0.25$ mag from photographic photometry of 48 RRab's in NGC 3201 by using the relation of Sturch (1966). In his compilation from the literature, Harris (1996) lists $E(B-V) = 0.21$ mag.[5] Gonzalez & Wallerstein (1998) obtained $E(B-V) = 0.25$ mag from a spectroscopic analysis of 18 red giants. The dust map of Schlegel et al. (1998) gives $E(B-V) = 0.24$ mag at the center of NGC 3201. Most recently, von Braun & Mateo (2001) quoted a mean $E(V-I) = 0.24$ mag [which corresponds to $E(B-V) \approx 0.20$ mag] from isochrone fits to their *VI* MSTO photometry.

The reddenings in Table 6 enable us to compute extinction corrections for each RRL independently. This is invaluable when the reddening varies significantly on small spatial scales as it does in NGC 3201. Figure 9 shows the extinction-corrected intensity-mean magnitudes plotted as a function of pulsation period. The reddening value for each RRc star in Table 6 and Figure 9 is the mean reddening from the three or four nearest RRab stars; statistics suggest they are accurate to $\sim$0.03 mag.

Several points are worth noting. First, the luminosity of the RRc stars appears to vary with pulsation period. The effect is most pronounced in *B*, less strong in *V*, and negligible in *I* (or perhaps the slope is in the opposite sense). However, this trend may be a spurious result of the small number of RRc's in NGC 3201, since the trend is not evident in the RRc's of the globular cluster M5 (Layden et al. 2003).

Second, for the RRab stars, the luminosity scatter is largest in *B*, smaller in *V*, and smaller still in *I*. This could be related to the larger extinction corrections applied in the bluer passbands. Nevertheless, the trend suggests that when estimating distances to objects in environments with strong and spatially variable reddening, observers should employ passbands with the longest possible wavelengths.

Third, the RRab *I*-band luminosities show a distinct correlation with wavelength. A least-squares fit yields the relation $\langle I\rangle_0 = -1.99P + 14.56$ (rms $= 0.06$), where $P$ is the pulsation period. This relation is reminiscent of the $M_K$-period relation (Longmore et al. 1990). When a precise distance is available for NGC 3201, the cluster will prove valuable in calibrating the $M_I$-period-metallicity relation.

Finally, the means of the extinction-corrected apparent magnitudes for the 58 RRLs in NGC 3201 are $\overline{B_0} = 14.259 \pm 0.015$ mag, $\overline{V_0} = 13.972 \pm 0.011$ mag, and $\overline{I_0} = 13.472 \pm 0.010$ mag. We discuss the distance implied by these apparent magnitudes in § 6.2.

Ultimately, we wish to deredden all the stars in the field to obtain the clearest possible impression of the cluster's CMD. Piersimoni et al. (2002) created a reddening map for NGC 3201 by fitting a slowly varying function to their $E(B-V)$ and $E(V-I)$ data as functions of $XY$ position. However, the spatial distribution of RRab's within NGC 3201 is very nonuniform, leaving large regions where no RRab's exist. In these regions, the fits are poorly

[5] Updated at http://physun.physics.mcmaster.ca/Globular.html, June 1999.

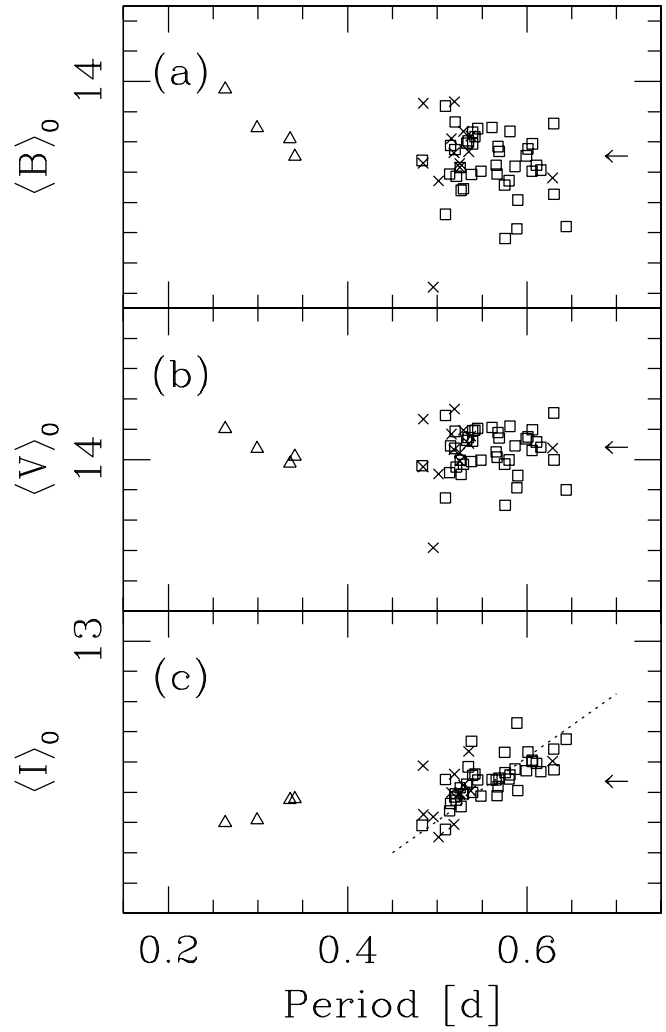


FIG. 9.—Extinction-corrected intensity-mean RRL magnitudes in the *B*, *V*, and *I* passbands as a function of pulsation period, showing RRc stars (*triangles*), RRab stars with complete light curves (*squares*), and RRab stars with significant gaps in phase coverage (*crosses*). Arrows indicate the mean magnitude in each passband. The dotted line marks the least-squares fit to the RRab stars in the *I*-band. In each plot, the minor tick marks on the *y*-axis are separated by 0.1 mag.

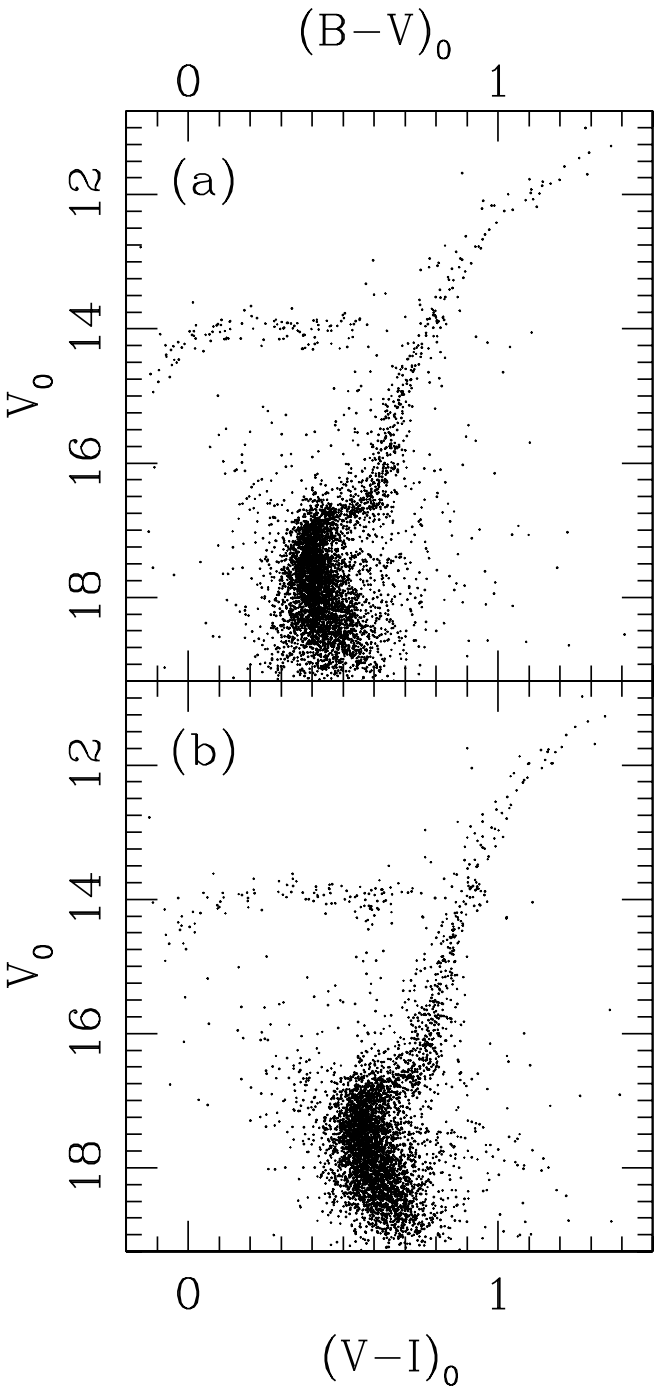


FIG. 10.—Dereddened CMDs of NGC 3201 (*a*) using the $E(B-V)$ values of 54 RRab stars and (*b*) using the $E(V-I)$ values of the same stars. In both plots, faint stars near the center of the cluster have been omitted to minimize scatter in the CMD.

constrained. We take a different approach. At the *XY* location of each star, we find the nearest RRab star. If the RRab is within 30″ of the star, we apply the reddening of the RRab to the star; if it is not, we omit the star from the dereddened CMD. Figure 10 shows the dereddened CMDs. The principal sequences are tighter than in Figure 2, indicating that we successfully reduced the influence of the spatially varying foreground reddening.

## 6. CLUSTER PROPERTIES

### 6.1. *Metallicity*

Our differentially dereddened CMDs provide us the opportunity to estimate the metallicity of NGC 3201 from the shape and location of the RGB by using the simultaneous reddening and metallicity (SRM) method of Sarajedini (1994). Using our $B-V$ CMD from Figure 10, we obtain $[\mathrm{Fe/H}] = -1.54 \pm 0.16$ and $E(B-V) = -0.03 \pm 0.05$. From our $V-I$ CMD and the SRM calibration in Sarajedini & Layden (1997), we obtain $[\mathrm{Fe/H}] = -1.89 \pm 0.16$ and $E(V-I) = 0.00 \pm 0.04$ [equivalent to $E(B-V) = 0.00 \pm 0.04$]. The weighted mean values are then $[\mathrm{Fe/H}] = -1.72 \pm 0.11$ and $E(B-V) = -0.01 \pm 0.03$.

The SRM reddening value is expected to be zero to within the errors, since it was derived from differentially dereddened data. The fact that it is zero underscores the systematic consistency of the SRM and RR Lyrae reddening techniques.

Our SRM metallicity estimate is in good agreement with the value $-1.61 \pm 0.12$ dex quoted by Zinn & West (1984), and in fair agreement with $-1.53 \pm 0.03$ dex from the compilation by Rutledge et al. (1997).[6] The SRM result seems to be slightly low, though the difference is less than $2\,\sigma$. Rather than reflecting a systematic difference between the SRM and other methods, we suspect the difference represents a random error. Despite our differential dereddening, the RGB of NGC 3201 remains slightly broaded by (1) residual star-to-star reddening differences and (2) misestimates of the true mean magnitudes of the RGB variables due to incomplete phase coverage. This broadening makes it less likely that the polynomial we fit to the observed RGB (as part of the SRM procedure) correctly represents the shape of the cluster's true RGB. In particular, the random misplacement of a few stars near the RGB tip can significantly affect the fitted curve. Since much of the metallicity information in the SRM method comes from the curvature of the RGB, a cluster with a broadened RGB is more likely to experience a random error in its metallicity estimate. We suspect that such a random error has occurred in our estimate of the metallicity of NGC 3201. Note that the reddenings derived from the SRM method are less susceptible to this effect, since the reddening information comes mainly from the mean color of the RGB, which is "anchored" by the large number of stars on the lower RGB.

### 6.2. *Distance*

In § 5, we determined the dereddened intensity-mean apparent magnitude for the 58 RRLs in our study. Converting these into a distance is complicated by uncertainties in the RRL absolute magnitude calibration. The most probable calibration from Chaboyer (1999) yields $M_V(\mathrm{RR}) = 0.58 \pm 0.12$ mag if we adopt $[\mathrm{Fe/H}] = -1.53$ on the Zinn & West (1984) scale (Rutledge et al. 1997), which in turn leads to a distance of $4.78 \pm 0.27$ kpc. The distance is 3% smaller if we adopt $[\mathrm{Fe/H}] = -1.24$ on the Carretta & Gratton (1997) scale (Rutledge et al. 1997) and 2% larger if we adopt our value of $[\mathrm{Fe/H}] = -1.72$ dex from the SRM method.

In § 4.3, we suggested that two stars, Nos. 752 and 1019, are probably $\delta$ Scuti star members of NGC 3201 and that three other stars may be DSSs as well (Nos. 651, 776, and 941). The $V$-band photometric amplitudes of Nos. 752 and 1019 are greater than 0.25 mag, qualifying them as high-amplitude DSSs. The properties of these radially pulsating variable stars are discussed by McNamara (1997) and references therein.

Various researchers have sought to derive a period-luminosity ($P$-$L$) relationship for high-amplitude DSSs (HADSs). Most recently, Petersen & Hog (1998) and McNamara (1997) used trigonometric parallaxes from the *Hipparcos* satellite to calibrate the zero point of the HADS $P$-$L$ relation. A note of caution is required, however, since only three HADSs contribute to these $P$-$L$ relations with high weight, and only one of those stars has a metallicity typical of the halo (SX Phoenicis, $[\mathrm{Fe/H}] = -1.4$ dex). In the following, we adopt the $P$-$L$ relation presented in equation (8) of Petersen & Hog (1998).

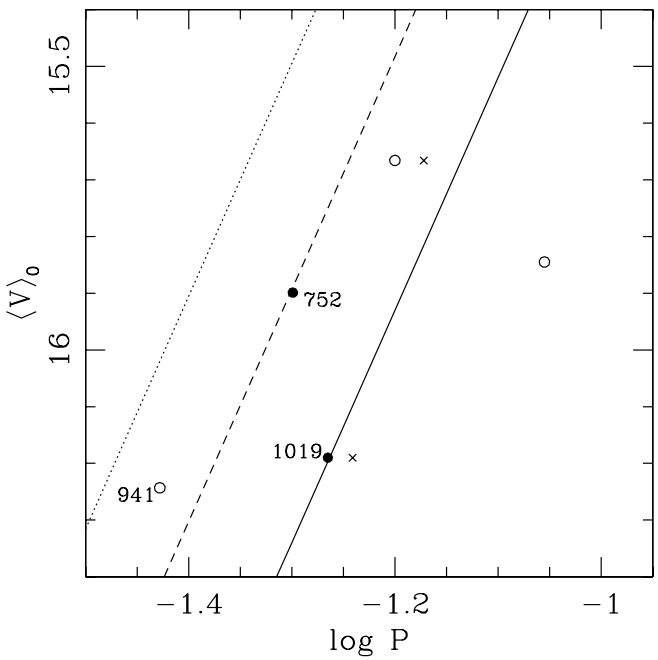


FIG. 11.—Dereddened intensity-mean $V$-band magnitude of each $\delta$ Scuti star candidate, plotted against the logarithm of the star's period, showing probable DSSs (*filled circles*), possible DSSs (*open circles*), and the alternate periods shown in Table 8 (*crosses*). The lines indicate the period-luminosity relation of Petersen & Hog (1998), shifted by a distance modulus of 13.35 mag. The solid line marks the locus of fundamental mode pulsators, while the dashed and dotted lines mark the loci of first- and second-overtone pulsators, respectively.

Figure 11 shows our five DSS candidates in a plot of dereddened, intensity-mean $V$-band magnitude versus the logarithm of the period. The solid line shows the $P$-$L$ relation presented in equation (8) of Petersen & Hog (1998), which is applicable to fundamental mode pulsators. The relations for first- and second-overtone pulsators (the dashed and dotted lines, respectively) were derived by shifting the fundamental mode relation by $P_1/P_0 = 0.778$ and $P_2/P_1 \approx 0.8$, respectively. The three lines were shifted vertically as a group to achieve a best match to the observed points. Though there is some ambiguity in which mode is expressed by which star, the fit to stars 752 and 1019 is excellent as shown, corresponding to a cluster distance modulus of 13.35 mag. Considering uncertainties in the reddening and photometric zero point, the observational uncertainty is about 0.04 mag, while the systematic uncertainty in the $P$-$L$ relation is about 0.1 mag (Petersen & Hog 1998). This corresponds to a distance of $4.67 \pm 0.24$ kpc, in excellent agreement with our RRL-based distance estimate of 4.78 kpc.

Figure 11 suggests that star 1019 pulsates in the fundamental mode, while No. 752 pulsates in the first overtone. Assuming it is a cluster member, star 941 is too bright to be a first-overtone pulsator, and too faint to pulsate in the second overtone. However, the photometric amplitude of No. 941 is below that of the strict definition of a HADS, so it may not follow the $P$-$L$ relation obeyed by the larger amplitude stars.

[6] Rutledge et al. 1997 presented two globular cluster metallicity scales, one calibrated to the metallicities of Zinn & West 1984 and one to those of Carretta & Gratton 1997. We compare our SRM-based metallicity estimate with the former, since the SRM method is calibrated to the Zinn & West 1984 scale. Our observation is not useful in selecting which calibration better represents the true metallicity of NGC 3201.

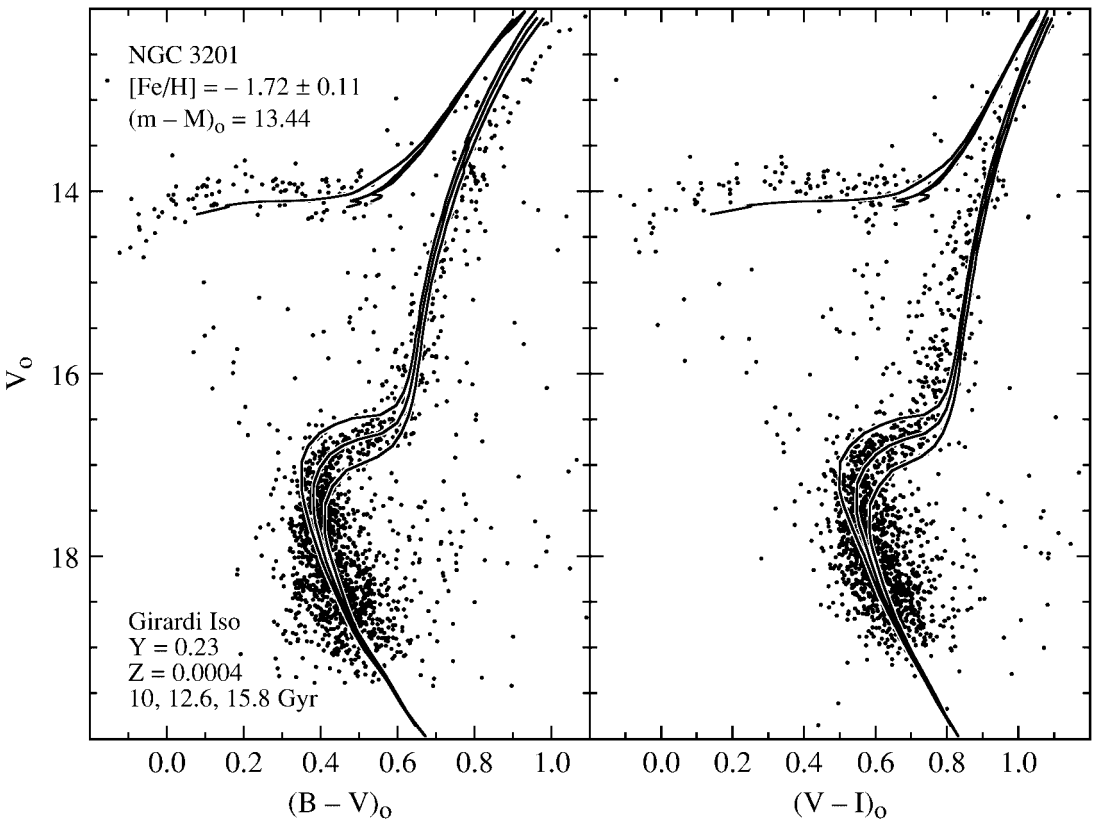


FIG. 12.—Dereddened CMDs from Fig. 10 with faint stars near the cluster center excluded to minimize photometric scatter around the MSTO region. Curves mark isochrones (Girardi et al. 2000) for [Fe/H] = −1.71, shifted by a distance modulus of $(m-M)_0 = 13.44$ mag. The isochrones ages are 10.0, 12.6, and 15.8 Gyr. The locus of stars near the MSTO suggests that NGC 3201 has an age of 13 ± 2 Gyr.

### 6.3. *Age*

One method by which we can investigate the age of NGC 3201 is via comparison with theoretical isochrones. In doing this, we follow the example of Melbourne et al. (2000) to allow a comparison of our results with theirs. We utilize the models of Girardi et al. (2000) for $Z = 0.0004$, which corresponds to [Fe/H] = −1.71 for a scaled solar chemical abundance mixture. For the distance modulus, we adopt the Chaboyer (1999) RR Lyrae luminosity scale, which predicts $M_V(\mathrm{RR}) = 0.53 \pm 0.12$ at the metal abundance of the adopted isochrones. Combining this with our observed mean level of the RRLs yields $(m-M)_0 = 13.44$ mag, in good agreement with our result derived from the $\delta$ Scuti stars in NGC 3201.

Figure 12 shows our dereddened CMDs for NGC 3201, where fainter stars near the cluster center have been excluded to minimize the effects of photometric scatter due to crowding. The theoretical isochrones are plotted after being shifted by the calculated distance modulus. No correction is made for the reddening because each star has already been extinction-corrected using the nearest RRL variable (see § 5). From these comparisons, we estimate an age of 13 ± 2 Gyr for NGC 3201. This value is in accord with the ages of M5 and M92 as measured by Melbourne et al. (2000) using identical procedures and models. If we employ isochrones with $Z = 0.001$ ([Fe/H] = −1.3), we obtain an age of 10 ± 2 Gyr.

Another age-dating technique that we have used successfully in the past (Layden & Sarajedini 2000; Melbourne et al. 2000) is the magnitude difference ($\Delta V_{\mathrm{SGB}}^{\mathrm{HB}}$) between the HB and the subgiant branch (SGB) at a point 0.21 mag bluer than $(V-I)_g$. We have previously applied this diagnostic to M5, M92, NGC 4833, and the globular clusters belonging to the Sagittarius dwarf galaxy (M54, Ter7, Ter 8, and Arp 2).

Using the NGC 3201 photometry shown in Figure 12, we construct a luminosity function of the SGB centered at $(V-I) = (V-I)_g - 0.21 = 0.69$ with a full width of 0.03 mag. A Gaussian function fitted to this luminosity function gives a peak magnitude of $V(\mathrm{SGB}) = 16.70 \pm 0.04$, which, when combined with our mean RRL magnitude, leads to $\Delta V_{\mathrm{SGB}}^{\mathrm{HB}} = 2.73 \pm 0.04$. Applying the Girardi et al. (2000) isochrone calibration of age in terms of $\Delta V_{\mathrm{SGB}}^{\mathrm{HB}}$ formulated by Melbourne et al. (2000), we find that NGC 3201 is 13.4 ± 0.5 Gyr old. Again, this compares favorably with the ages of M5 (13.4 ± 0.6 Gyr) and M92 (13.8 ± 0.6 Gyr) estimated by Melbourne et al. (2000) using the same age diagnostic and theoretical models. If we use isochrones for $Z = 0.001$, we obtain an age of 12.4 ± 0.7 Gyr. In either case, our result does not support the abnormally old age of 18 Gyr, which von Braun & Mateo (2001) found provided the best fit to their deep $V-I$ photometry. NGC 3201 appears to have formed at a time typical of other Galactic globular clusters of its abundance.

## 7. CONCLUSIONS

We have presented new time series photometry of the Galactic globular cluster NGC 3201 in the *BVI* passbands.

We derived high-quality light curves for 58 RRLs in the cluster. The queue-scheduled observing mode by which our data were obtained provided a time sampling that resulted in unusually gap-free light curves. Our light-curve parameters are in good agreement with those of Piersimoni et al. (2002).

We confirmed the debated variability of the red giant star V79 and detected low-level (0.01 to 0.1 mag) variability in at least 20 other red giants in the direction of NGC 3201. These stars appear to be low-metallicity globular cluster equivalents of the SARV field stars discussed by Percy et al. (2001) and references therein. Long-term monitoring of these stars is required to fully analyze their pulsation properties.

Among the fainter stars in our survey, we detected and confirmed the variability of eclipsing binary stars discussed by von Braun & Mateo (2002). We also discovered several $\delta$ Scuti (SX Phoenicis) type variables that appear to be members of NGC 3201. Using the period-luminosity relation of Petersen & Hog (1998) with the observed properties of the two best candidates, we obtained a heliocentric distance of $4.67 \pm 0.24$ kpc for NGC 3201.

We used the observed colors of our RRLs together with the relations of Blanco (1992) and Day et al. (2002) to estimate the interstellar reddening toward each RRL on a star-by-star basis. The mean reddening for the RRLs within $2'.0$ of the cluster center is $E(B-V) = 0.25$ and $E(V-I) = 0.34$ mag. After dereddening each RRL, we obtained a mean apparent magnitude of $\langle V \rangle_0 = 13.97$ mag for the RRLs in the cluster. Together with the RRL absolute magnitude advocated by Chaboyer (1999), this yields a distance of $4.78 \pm 0.27$ kpc. The star-to-star scatter among the dereddened RRL apparent magnitudes is small (rms = 0.08 mag), underscoring the value of these Population II standard candles, at least at a fixed chemical composition. The agreement between the distances estimated from RRL and $\delta$ Scuti stars is impressive.

We created a dereddened CMD of NGC 3201 by adopting for each nonvariable star the reddening value of the nearest RRL, provided it was within $30''$. We used this CMD, together with the isochrones of Girardi et al. (2000), to estimate the age of NGC 3201 at $13.4 \pm 0.5$ Gyr. This value is typical of other Galactic globular clusters at this metallicity.

Our results for the reddening, distance, metallicity, and age of NGC 3201 were shown to be internally consistent and are tied to the metallicity scale of Zinn & West (1984). The relevant relationships would need to be recalibrated if one were to adopt the metallicity scale of Carretta & Gratton (1997). Our results underscore the effectiveness of deriving reddening and distance information from the light curves of RRLs, particularly in environments where the reddening is high and spatially variable.

The authors appreciate the helpful comments of Ted von Hippel and an anonymous referee. This project was funded by the National Science Foundation through grant AST 99-88259 and made use of the Astrophysics Data System Abstract Service.

## APPENDIX

## NOTES ON VARIABLE STARS

Clement et al. (2001) list the following variable stars in NGC 3201 as "not variable": V33, V70, V74, V75, V79, and V82. With one exception, our photometry confirms this finding: the variability index (Stetson 1994) is consistent with other nonvariable stars and is a factor of at least 13 times smaller than for the least variable RRL. Our photometry also shows V97 and V99, i.e., stars 1103 and 2403 of Lee (1977), to be nonvariable at a similar level. However, we do detect low-level variability in the RGB tip star V79 (see § 4.2).

## REFERENCES

Blanco, V. M. 1992, AJ, 104, 734
Cacciari, C. 1984, AJ, 89, 231
Cardelli, J. A., Clayton, G. C., & Mathis, J. S. 1989, ApJ, 345, 245
Carretta, E., & Gratton, R. G. 1997, A&AS, 121, 95
Carretta, E., Gratton, R. G., Clementini, G., & Fusi Pecci, F. 2000, ApJ, 533, 215
Chaboyer, B. 1999, in Post-*Hipparcos* Cosmic Candles, ed. A. Heck & F. Caputo (Dordrecht: Kluwer), 111
Chaboyer, B., Demarque, P., Kernan, P. J., & Krauss, L. M. 1998, ApJ, 494, 96
Clement, C. M., et al. 2001, AJ, 122, 2587
Cool, A. M., Piotto, G., & King, I. R. 1996, ApJ, 468, 655
Day, A. S., et al. 2002, PASP, 114, 645
Eggen, O. J. 1977, ApJ, 213, 767
Girardi, L., Bressan, A., Bertelli, G., & Chiosi, C. 2000, A&AS, 141, 371
Gonzalez, G., & Wallerstein, G. 1998, AJ, 116, 765
Harris, W. E. 1996, AJ, 112, 1487
Landolt, A. U. 1992, AJ, 104, 340
Layden, A. C. 1994, AJ, 108, 1016
Layden, A. C., Cool, A., von Hippel, T., & Sarajedini, A. 2003, in preparation
Layden, A. C., & Sarajedini, A. 2000, AJ, 119, 1760
Lee, S.-W. 1977, A&AS, 28, 409
Longmore, A. J., Dixon, R., Skillen, I., Jameson, R. F., & Fernley, J. A. 1990, MNRAS, 247, 684
McNamara, D. H. 1997, PASP, 109, 857
Melbourne, J., Sarajedini, A., Layden, A. C., & Martins, D. H. 2000, AJ, 120, 3127
Percy, J. R., Wilson, J. B., & Henry, G. W. 2001, PASP, 113, 983
Perryman, M. A. C. 2002, Ap&SS, 280, 1
Petersen, J. O., & Hog, E. 1998, A&A, 331, 989
Piersimoni, A. M., Bono, G., & Ripepi, V. 2002, AJ, 124, 1528
Preston, G. W. 1959, ApJ, 130, 507
Renzini, A., et al. 1996, ApJ, 465, L23
Rutledge, G. A., Hesser, J. E., & Stetson, P. B. 1997, PASP, 109, 907
Sarajedini, A. 1994, AJ, 107, 618
Sarajedini, A., & Layden, A. C. 1997, AJ, 113, 264
Scargle, J. D. 1982, ApJ, 263, 835
Schlegel, D. J., Finkbeiner, D. P., & Davis, M. 1998, ApJ, 500, 525
Smith, H. A. 1995, RR Lyrae Stars (Cambridge: Cambridge Univ. Press), 91
Stetson, P. B. 1987, PASP, 99, 191
———. 1994, PASP, 106, 250
———. 2000, PASP, 112, 925
Sturch, C. 1966, ApJ, 143, 774
Unwin, S. 2000, in IAU Symp. 202, Planetary Systems in the Universe, ed. A. Penny, P. Artymowicz, A.-M. Lagrange, & S. Russell (San Francisco: ASP), 112
von Braun, K., & Mateo, M. 2001, AJ, 121, 1522
———. 2002, AJ, 123, 279
Zinn, R., & West, M. J. 1984, ApJS, 55, 45